AN ABSTRACT OF THE THESIS OF

Terry Chriss for the degree of Doctor of Philosophy

in Oceanography presented on September 4, 1981

Title: A Study of Turbulence in the Viscous Sublayer and Logarithmic Region of the Bottom Boundary Layer

Redacted for privacy

Abstract approved: D. R. Caldwell

Detailed current profiles between the sediment-water interface and 20 cm above it reveal a viscous sublayer in the bottom boundary layer on the Oregon continental shelf. Data from three field experiments are used to test fundamental assumptions about boundary layer flow in the ocean. The first study, discussed in Chapter 1, evaluates the hypothesis that, in the absence of the obvious influence of topographic irregularities, the flow behaves like a universally similar, neutrally-buoyant flow over a smooth wall. The second study, discussed in Chapter 2, evaluates the influence which irregular small-scale topography may have on the near-bed flow, while the third, discussed in Chapter 3, examines streamwise velocity fluctuations in the viscous sublayer and buffer layer and evaluates the hypothesis that spectra from the viscous sublayer and buffer layer of laboratory and geophysical boundary layer flows can be reduced to universal forms.

Although the thickness of the viscous sublayer scales with ν/u_* as required by universal similarity, the non-dimensional sublayer thickness is not as constant as in neutrally-buoyant laboratory flows. Even in the absence of the obvious effects of bottom irregularities, the near-bed flow is not as simple as smooth-walled boundary-layer flows in the laboratory. In the second study, it is shown that when the near-bed flow experiences resistance due to form drag as well as skin friction, the constant stress boundary layer assumption is not valid close to the sediment-water interface. In the third study, it is shown that non-dimensionalized spectra of streamwise velocity fluctuations in the viscous sublayer and buffer layer at the ocean floor are very similar to those found in the laboratory.

A Study of Turbulence in the Viscous Sublayer and Logarithmic Region of the Bottom Boundary Layer

by

Terry Michael Chriss

A THESIS

submitted to

Oregon State Univesity

in partial fulfillment of
the requirements for the
degree of

Doctor of Philosophy

June 1982

APPROVED:

Redacted for privacy

Professor of Oceanography in charge of major

Redacted for privacy

Associate Dean of Oceanography

Redacted for privacy

Dean of Graduate School

Date thesis is presented September 4, 1981

Typed by Pam Wegner for Terry Chriss

ACKNOWLEDGEMENTS

Particular thanks are expressed to my advisor, Doug Caldwell, who conceived of the original experiment and designed a major portion of the instrumentation. I sincerely appreciate the freedom he allowed me in running the experiments and in the data analysis, together with the fact that he always seemed to have a solution when problems arose.

I would also like to express my appreciation to Paul Komar, Vern Kulm, and George Keller who supported me (both financially and otherwise) during my first few years at OSU, when it sometimes seemed as if funds for my research would never be forthcoming.

This research was made possible because of the help, dedication, and long hours put in by a number of individuals. Particular appreciation is expressed to Mark Matsler (profiler and tripod development), Steve Wilcox (electronics design), Stuart Blood (software development), Mike Brown (sensor construction), and Milo Clauson (camera development and general counsel). Ralph Moore and Bob Schum spent many hours calibrating and assembling sensors, and Stuart Eide and Tom Dillon generously supplied advice and assistance in the laboratory. The above individuals (and many others) supplied able assistance at sea, and the captain and crew of the research vessel WECOMA were extremely helpful in accomodating a complex mooring procedure. Special appreciation is expressed to Priscilla Newberger who calibrated electronics, helped run some of the experiments at sea, and generously gave of her time to discuss and evaluate this research.

Finally, my love and appreciation is expressed to my wife, Heidi, and my son, Ian, both of whom sacrificed a great deal so that this work could be completed.

TABLE OF CONTENTS

Chapter I

Universal Similarity and the Thickness of the Viscous Sublayer at the Ocean Floor 1
Abstract 2
Introduction 3
Theoretical Background 4
The Experiment 10
Data Analysis 12
Discussion 19
Conclusions 41

Chapter II

Evidence for the Influence of Form Drag on Bottom Boundary Layer Flow 43
Abstract 44
Introduction 45
The Experiment 51
Data Analysis 53
Discussion 56
Conclusions 71

Chapter III

Turbulence Spectra from the Viscous Sublayer and Buffer Layer at the Ocean Floor 73
Abstract 74
Introduction 75
The Experiment 76
Data Analysis 78
Spectra from the Viscous Sublayer 81
The Vertical Structure of the Streamwise Velocity Fluctuations in the Viscous Sublayer 98
Spectra from the Buffer Layer 99
Discussion 106
Conclusions 116

References 117

LIST OF FIGURES

Figure		Page
Chapter I		
I-1	Theoretical mean velocity profile for a logarithmic layer above a viscous sublayer	8
I-2	Typical near-bed velocity profile for the June 1979 experiment	14
I-3	As in I-2 but with a logarithmic scale for the distance above the sediment	16
I-4	The thickness of the viscous sublayer plotted against the quantity ν/u_*	21
I-5	The relationship between the measured velocity at 59 cm above the bed and that calculated from u_* and the assumption of a non-dimensional sublayer thickness of 11.1	24
I-6	The relationship between the measured velocity at 59 cm above the bed and that calculated from u_* and the measured sublayer thickness	26
I-7	The measured non-dimensional sublayer thickness plotted against the sublayer thicknesses "required" by the rotor data	29
I-8	Non-dimensional plot of all of the mean velocity data from our study	32
I-9	Non-dimensional plot of the mean velocity data from laboratory boundary layer experiments (reprinted from Monin and Yaglom, 1971)	34
I-10	Non-dimensional mean velocity profiles for three selected intervals from our study	36
Chapter II		
II-1	Typical mean velocity profile for the October 1978 experiment	48

LIST OF FIGURES (cont.)

Figure		Page
II-2	As in II-1 but with an expanded scale which emphasizes the logarithmic regions of the velocity profile	50
II-3	Bottom photograph representative of those obtained 65 km south of our studied area, from a region of the same water depth	64
II-4	Additional bottom photograph, as in II-3	66
Chapter III		
III-1	Typical time series for the viscous sublayer and buffer layer	80
III-2	Typical mean velocity profile for the viscous sublayer and buffer layer	83
III-3	Typical spectra from the viscous sublayer	86
III-4	Sublayer spectra from this study plotted with laboratory spectra from Blakewell and Lumley (1967) and Ueda and Hinze (1975)	89
III-5	Non-dimensional sublayer spectra from the above laboratory studies	93
III-6	Non-dimensional sublayer spectra from the present study plotted with the non-dimensional spectra from the laboratory studies	95
III-7	Ensemble-averaged spectrum from the present study plotted with the laboratory spectra	97
III-8	Representative buffer layer spectra from the present study plotted with laboratory buffer layer spectra from Blakewell and Lumley (1967) and Ueda and Hinze (1975)	102
III-9	Scaled buffer layer spectra from the above laboratory studies	104
III-10	Scaled buffer layer spectra from the present study plotted with the laboratory spectra of Figure III-9	108

LIST OF FIGURES (cont.)

Figure		Page
III-11	Ensemble-averaged buffer layer spectrum from the present study plotted with the scaled laboratory spectra	110
III-12	Buffer layer spectra for two 1024-point series from the present study plotted with the scaled laboratory spectra	115

LIST OF TABLES

Table		Page
1	Friction velocities, roughness lengths, and von Karman's constants for the individual data intervals	55
2	Estimated distances from sensor to roughness elements	58
3	Estimated roughness element heights	61
4	Ratio of the total stress to the bed stress as well as drag coefficients for the individual data intervals	70

A STUDY OF TURBULENCE IN THE VISCOUS SUBLAYER AND LOGARITHMIC REGION OF THE BOTTOM BOUNDARY LAYER

CHAPTER I

UNIVERSAL SIMILARITY AND THE THICKNESS OF THE VISCOUS SUBLAYER AT THE OCEAN FLOOR

T. M. Chriss

School of Oceanography

Oregon State University

Corvallis, Oregon 97331

ABSTRACT

Experiments conducted on the Oregon continental shelf in June 1979 indicate that the boundary layer flow at the sea floor was hydrodynamically smooth. Fine-resolution velocity profiles are used to test the assumption that the flow behaved like a universally-similar, neutrally-buoyant flow over a smooth wall. Although estimates of von Karman's constant ($0.43 \pm .05$) are consistent with values from laboratory and atmospheric boundary layers, the non-dimensional thickness of the viscous sublayer is more variable than in laboratory studies. Because the flow is not as simple as implied by universal similarity, bed stress estimates using the commonly cited equations which are based on universal similarity may not always yield accurate results.

INTRODUCTION

The simplest model that might describe the flow near the sea bed is provided by laboratory studies of neutrally stratified turbulent boundary layers (Monin and Yaglom, 1971; Townsend, 1976; Yaglom, 1979). This model is specially appealing because the concept of universal similarity seems to apply to these flows. The concept suggests that experimental results, when expressed in an appropriate non-dimensional form, are independent of flow conditions and fluid properties. Thus, profiles of mean velocity and other flow variables become "universal" when velocity measurements are non-dimensionalized by an appropriate velocity scale, and when distances from the boundary are non-dimensionalized by an appropriate length scale.

In an earlier paper (Caldwell and Chriss, 1979), we demonstrated, for the first time, the existence of a viscous sublayer in the near-bed flow in the ocean. A later, more detailed examination of additional data from that experiment revealed a "kink" in the profiles 11-15 cm above the bed. We concluded that the flow above the kink was significantly influenced by form drag due to topographic irregularities (Chriss and Caldwell, 1981a). Although the flow was "hydrodynamically smooth" in the sense that a viscous sublayer was always present, the true bed stress (computed from the velocity profile in the viscous sublayer) was several times smaller than the stress computed from the portion of the velocity profile influenced by form

drag. A subsequent experiment (June 1979) confirms the existence of a viscous sublayer but data analysis (later in this paper) indicates no measurable influence of form drag on the flow. We might, then, picture the near-bed flow as closely resembling laboratory flows over a smooth wall, but sometimes being perturbed by the effects of small-scale topography.

Because the data from June 1979 show no obvious influence of topographic irregularities, we use it to examine the hypothesis that, in the absence of such influence, the flow can be appropriately described as a universally similar, neutrally-buoyant boundary layer flow on a smooth wall. Data gathered during this experiment will be used to test the applicability of the assumptions that lead to the conventional equations for such flows. This question is far from academic. Papers dealing with sediment transport and boundary layer processes (e.g. Bowden, 1978; Wimbush and Munk, 1971; Komar, 1976) often cite equations which imply that, if a viscous sublayer exists, the flow behaves like universally similar, neutrally-buoyant flows over a smooth wall. We find that, even in the absence of form drag effects, the very near-bed flow is not quite so simple and that bed stress estimates based on the assumption of universal similarity may not always be accurate.

THEORETICAL BACKGROUND

This development follows Monin and Yaglom (1971, chapter 3), recasting slightly to emphasize the significance of the viscous sublayer. Given that a viscous sublayer exists in which the molecular

viscosity, ν, dominates the vertical transport of momentum, the stress at the wall, τ_o, is given by:

$$\tau_o = \rho\nu \frac{\partial \bar{U}}{\partial z} \tag{1}$$

where ρ is the density of the fluid and $\bar{U}$ is the mean velocity at a distance z from the wall. Defining the friction velocity

$$u_* = (\tau_o/\rho)^{1/2} \tag{2}$$

and integrating (1) yields an expression for the velocity profile in the viscous sublayer

$$\bar{U}(z) = u_*^2 z/\nu \tag{3}$$

In the constant stress portion of the overlying turbulent logarithmic layer, the shear is given by

$$\frac{\partial \bar{U}}{\partial (\ln z)} = u_*/k \tag{4}$$

which defines von Karman's constant, k. Integrating (4), we obtain

$$\bar{U}(z) = (u_*/k) \ln z + C \tag{5}$$

where C is a constant of integration whose value is still to be determined. Defining the sublayer thickness, δ, by the point where the extrapolated sublayer profile (3) and the logarithmic velocity profile (5) intersect, we obtain:

$$u_*^2 \delta/\nu = (u_*/k) \ln \delta + C \tag{6}$$

Therefore, the constant of integration C is explicitly a function of the thickness of the viscous sublayer, δ, and is given by:

$$C = u_*^2 \delta/\nu - (u_*/k) \ln \delta \tag{7}$$

Thus, for the logarithmic portion of the turbulent boundary layer,

$$\bar{U}(z) = (u_*/k) \ln (z/\delta) + u_*^2\delta/\nu \qquad (8)$$

This form of the logarithmic profile equation demonstrates that the mean velocity within the logarithmic layer above a smooth wall depends not only on u_* but also on the sublayer thickness (Fig. 1).

Defining the non-dimensional distance from the wall, z^+, the non-dimensional sublayer thickness, δ^+, and a non-dimensional mean velocity, U^+, by $z/(\nu/u_*)$, $\delta/(\nu/u_*)$, and $\bar{U}/u_*$, respectively, we obtain

$$U^+ = (1/k) \ln (z^+/\delta^+) + \delta^+ \qquad (9)$$

If k and δ^+ are "universal constants," then this simple equation defines the logarithmic portion of all neutrally-buoyant turbulent boundary layer flows over a smooth wall.

At this point it is important to clarify the relationship between (9), and the commonly cited non-dimensional equation for the turbulent logarithmic layer over a smooth wall (Monin and Yaglom, 1971, p. 276-277):

$$U^+ = A \ln z^+ + B \qquad (10)$$

Comparison of (9) and (10) demonstrates that B is related to δ^+ by

$$B = -A \ln \delta^+ + \delta^+ \qquad (11)$$

Laboratory studies demonstrate that A and B do not vary significantly with fluid properties or flow conditions, thus lending support to universal similarity (Monin and Yaglom, 1971, p. 277). The most reliable data (Monin and Yaglom, 1971; Yaglom, 1979) indicate that A

Figure I-1. Theoretical mean velocity profile for a logarithmic layer overlying a viscous sublayer. Note that a logarithmic scale has been used for the distance from the boundary.

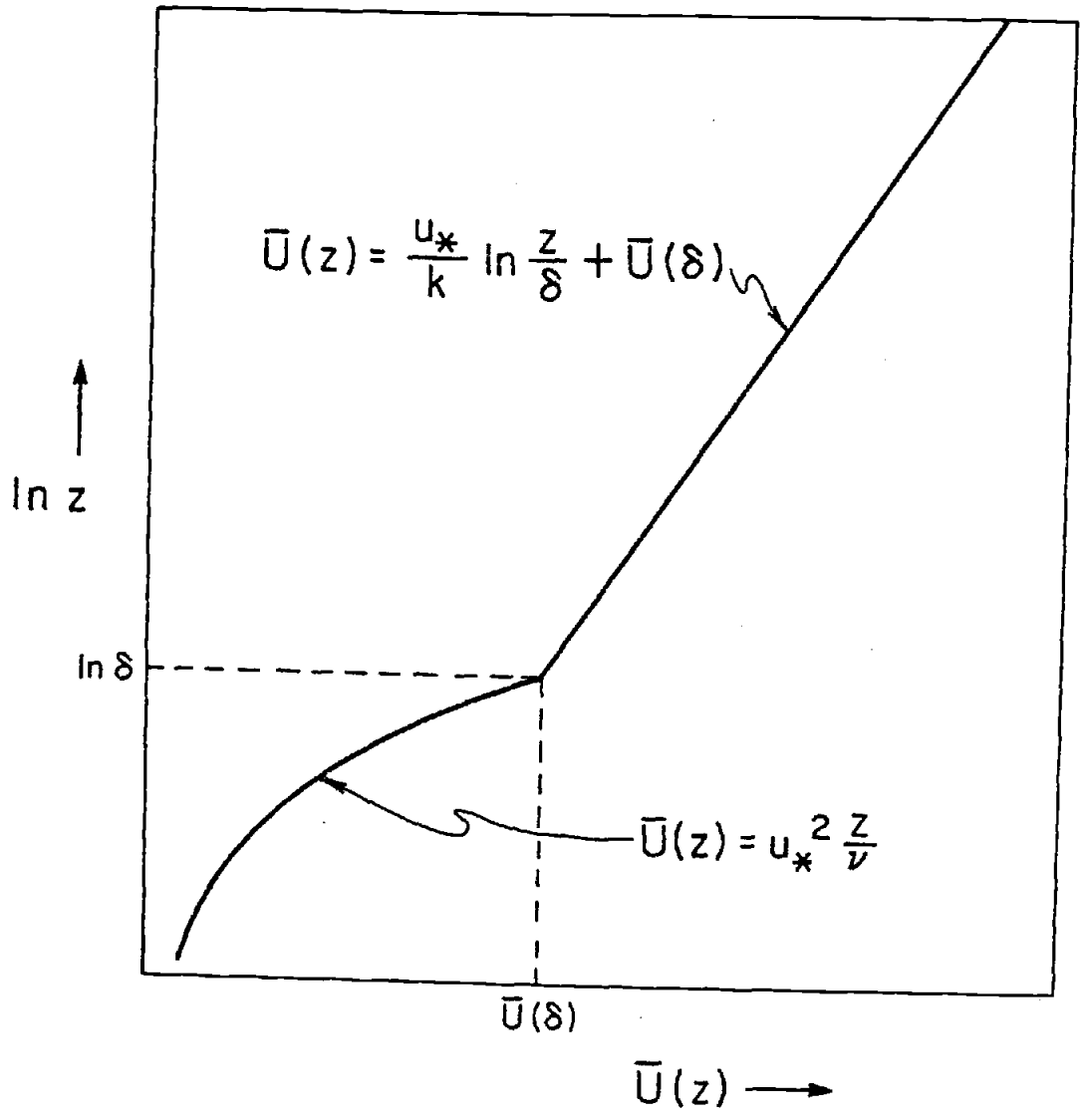
$\bar{U}(z) = \frac{u_*}{k} \ln \frac{z}{\delta} + \bar{U}(\delta)$
ln z
ln δ
$\bar{U}(z) = u_*^2 \frac{z}{\nu}$
$\bar{U}(\delta)$
$\bar{U}(z)$

Figure I-1.

is close to 2.5 (corresponding to a von Karman's constant of 0.4) and that B is 5 to 5.5. (While various investigators cite slightly different values for A and B, the differences are small. They are usually attributed to measurement errors or to differences in the z^+ range used for determining A and B. It should be clear from (11) that universal similarity requires that the non-dimensional sublayer thickness δ^+ be constant and that its value be between 11 and 11.6 (corresponding to B = 5 to 5.5). Because the difference between δ^+ = 11.1 and δ^+ = 11.6 reflects itself as a change of at most 2 percent in $\bar{U}(z)$, the differences between these two values is virtually insignificant. We will arbitrarily refer to the non-dimensional sublayer thickness of laboratory experiments as being 11.1 even though some workers cite slightly different values. We emphasize that this value, like equation (11), is based on operationally defining the sublayer thickness by the intersection of the extrapolated linear and logarithmic velocity profiles. In doing so, δ^+ includes not only the "true" viscous sublayer (the linear velocity profile region), but also a portion of the "buffer" region in which molecular viscosity and turbulence both contribute significantly to the vertical transport of momentum.

The data obtained during our experiments represent, to the best of our knowledge, the only velocity measurements obtained within the viscous sublayer of a geophysical boundary layer flow. Determinations of k and δ^+ permit us to evaluate the extent to which this geophysical boundary layer flow can be described as a universally similar, neutrally-buoyant turbulent flow over a smooth wall.

THE EXPERIMENT

The experiment was carried out between June 5 and June 13, 1979 in 90 m and 185 m water depth at 45°20'N on the Oregon shelf. The surface sediment at the 90 m station is a fine sand whereas at the 185 m station it is a silty sand (Runge, 1966). The data were obtained from profiling heated-thermistor velocity sensors mounted on a 2 m high tripod on the sea floor. Most data come from two deployments at the 185 m station. Some additional data were obtained during a deployment at the 90 m station. A data acquisition system on the tripod sampled each thermistor at an interval set from 2 seconds to 4 seconds depending on the deployment duration, 1 to 3 days. Additional instrumentation included profiling and stationary temperature sensors, Savonius rotors, a 25 cm path-length beam transmissometer, a high-resolution pressure transducer, and a time-lapse motion picture camera which monitored the condition of the sensors.

Current was supplied to each heated thermistor to heat it approximately 20°C above the water temperature. Because the velocity calibration is a function of both the water temperature and the orientation of the flow with respect to the thermistor, each thermistor was post-calibrated at the temperatures and flow directions observed during the experiment. Calibrations were performed by towing them in a 1 m radius annular channel, fitting to the formula

$$P/\Delta T = a + b\,U^N \qquad (12)$$

where P is the power dissipated in the thermistor, ΔT is its temperature rise, U is the speed, and a, b, and N are experimentally deter-

mined. Inversion of this formula allows the calculation of speed from measurements of $P/\Delta T$, which is computed from the output of a bridge circuit. Using (12) with empirically-determined a, b, and N, speed can be determined within 0.1 cm/s in the laboratory. The heated thermistors measure speed only, flow direction is determined by a small vane.

The heated thermistors were carried up and down by a crank-and-piston mechanism driven by an underwater motor. The profiling thermistors and the profiler mechanism was mounted outside one tripod leg, assuring unobstructed flow through an arc of 300 degrees. Only cases of unobstructed flow were chosen for analysis. The profiling period for these experiments was either one minute or ten minutes. The profiler period was optimized to measure temperature gradients within the viscous sublayer. The vertical travel of the sensors was 6 cm. To make sure that the thermistors penetrated the viscous sublayer (which at most a few cm thick), we allowed the thermistors to penetrate the sediment. The vertical position of the thermistors was determined from the output of a potentiometer connected to the profiler motor. Calibration of the profiler system showed that vertical position of the sensors can be determined within 0.03 cm. The position of the sediment-water interface was taken to be the zero-velocity intercept of the linear velocity profile in the viscous sublayer.

The Savonius rotor used in the data analysis was calibrated in the tow facility at the Bonneville Dam laboratory of the U.S. Army Corps of Engineers. The standard error of the calibration equation

is 0.33 cm/s.

DATA ANALYSIS

Mean velocity profiles were constructed by averaging over time intervals 9 to 133 minutes long, each interval containing multiple traverses. With a few exceptions, discussed later, intervals were chosen for steadiness of speed and direction. The lower portion of each traverse was divided into segments 0.1 cm thick for averaging, and the mean for each was determined by averaging all measurements within it during the repeated traverses. A typical averaged profile is shown in Figure 2 in which the linear profile just above the sediment again demonstrates the existence of a viscous sublayer. A semi-logarithmic plot of the same data (Fig. 3) indicates that the upper section is consistent with the assumption of a turbulent logarithmic layer. (In the logarithmic layer the velocity data has been averaged over 0.3 cm intervals.) The shear in the viscous sublayer was determined by linear regression, and the bed stress and the friction velocity were computed using (1) and (2). The kinematic viscosity, ν, for use in (1) was obtained from standard tables.

Velocity sensors sometimes malfunctioned (due to sea water leakage) or were broken during recovery. We allowed for these contingencies by using several sensors and always recovered at least one functioning sensor for post-calibration. We have compared the data from two thermistors separated horizontally by 11 cm during one of the 185 m deployments. In six of ten intervals, the velocity profiles from the two agree closely, the average difference between u_* values

Figure I-2. Typical mean velocity profile for the June 1979 experiment. The lowermost straight line represents a linear fit to the points in the viscous sublayer whereas the uppermost line represents a fit to the points in the lower portion of the logarithmic layer.

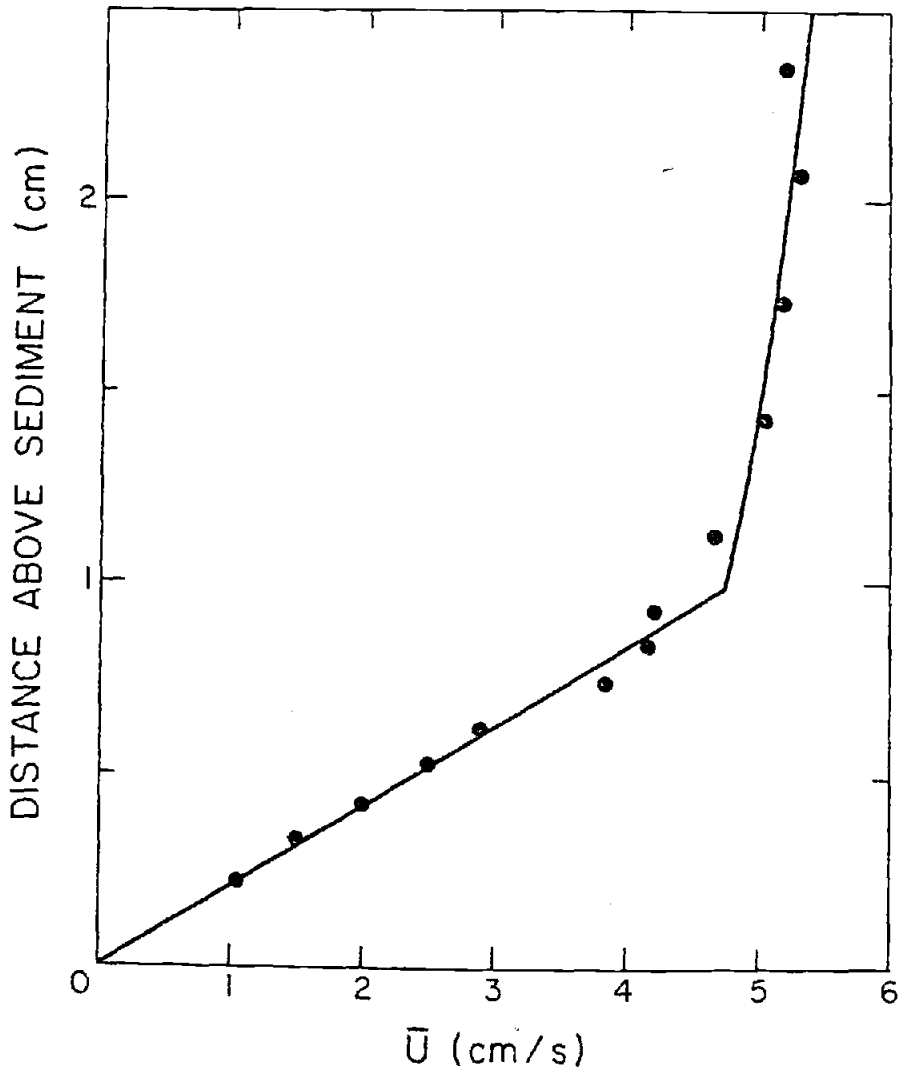

Figure I-2.

Figure I-3. Same data as in Figure 2 but plotted with a logarithmic scale for the distance above the sediment.

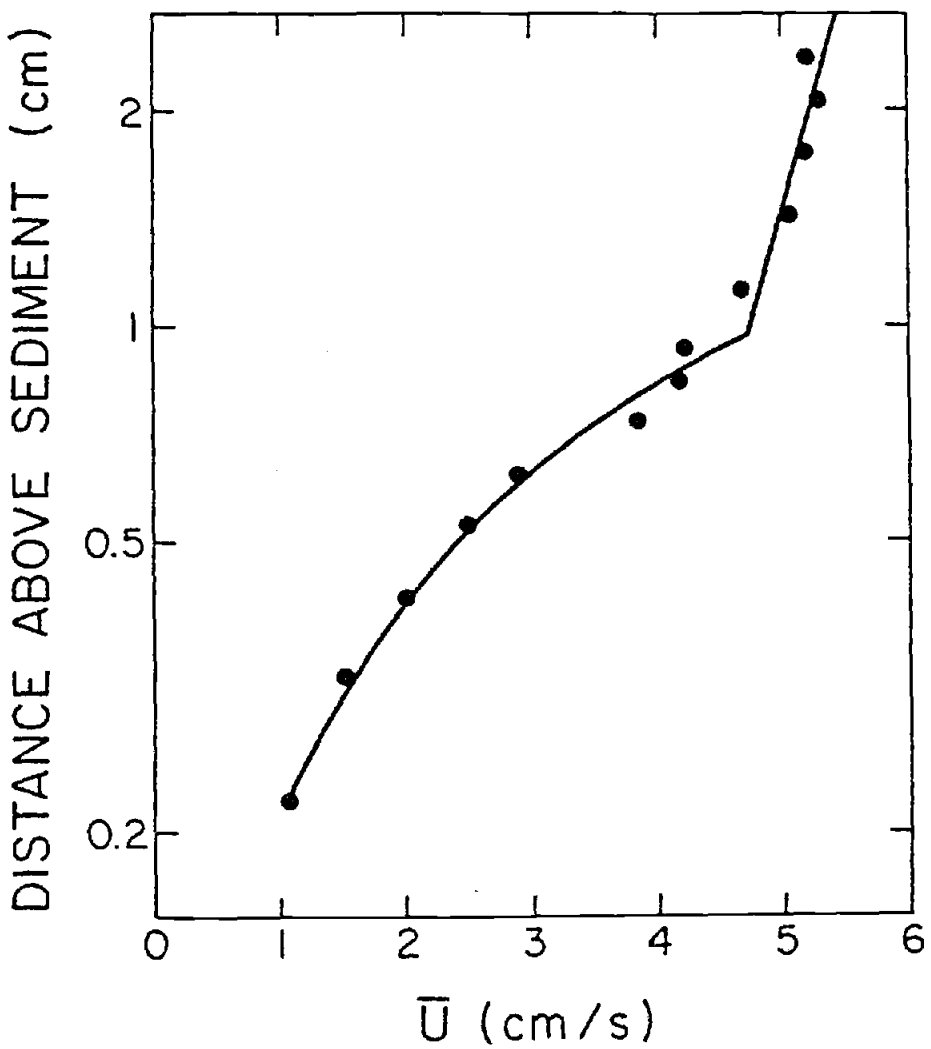

Figure I-3.

being only 3 percent. The four remaining intervals show an average difference of 25 percent. Although these four profiles do not agree in the sublayer, they agree very well above, suggesting that the differences may reflect real differences in the near-bed flow rather than sensor malfunction. If the differences are caused by sensor malfunction, the malfunctions must have been episodic, for these intervals are bounded by others in which the two sensors agree closely. We conjecture that the near-bed differences in the flow, if real, could have been the result of tiny topographic irregularities, their influence being limited to flow from certain directions. Because the resolution of our bottom photography is inadequate show such features and because the only arguments favoring sensor malfunction are that the two sensors do not agree, we have chosen to present the data from both sensors in the four cases in which they differ. It should be noted that inclusion of the data from both sensors in the following analysis does not significantly affect the conclusions of this study.

Estimation of von Karman's constant

Given u_* (from the sublayer profile) and the shear in the logarithmic layer, one can solve (4) for k. Because the traverse was limited to 6 cm in order to increase resolution in the viscous sublayer and because the thermistors penetrated the sediment at the bottom of the profile, enough of the logarithmic layer was not always covered for accurate determination of the shear (and hence k) using heated thermistor data alone. For this reason, we have determined

the log-layer shear by using the mean velocity from the top of the traverse together with the mean velocity from the Savonius rotor 59 cm above the sediment. This method of estimating k is not ideal in that it depends on measurements from two different sensors rather than from a single profiling sensor, nevertheless the average value of k based on a large number of these determinations is not likely to be significantly in error. From 23 individual velocity profiles we estimate k to be 0.43 $\pm$ 0.05 (95% confidence interval for the mean). This estimate compares favorably with an estimate of 0.419 $\pm$ 0.013 from a turbulent Ekman layer in the laboratory (Caldwell et al., 1972), as well as with a summary of atmospheric estimates which suggests a value of 0.41 $\pm$ 0.025 (Garrett, 1977). (Five velocity profiles were excluded from our analysis because the current speed was below the rotor threshold.) The confidence interval of our estimate depends on the standard deviation (0.11) of the 23 individual measurements of k and is not unreasonably large considering the accuracy of typical bottom boundary layer flow measurements. For example, for typical conditions during this experiment ($u_* \simeq .25$), an error of 0.4 cm/s in the measured rotor velocity would result in an error of approximately 0.07 in k. Considering the standard error of the rotor calibration (0.33 cm/s) as well as the problems involved in using Savonius rotors in the ocean, the standard deviation (0.11) is not surprising.

In summary, this estimate (0.43) of von Karman's constant in the bottom boundary layer is not significantly different from the value (k = 0.4) typically cited in laboratory studies. Thus this aspect of

the geophysical flow is consistent with the hypothesis that the flow is a universally similar, neutrally-buoyant flow on a smooth wall.

The thickness of the viscous sublayer

As discussed earlier, one of the implications of universal similarity is that the non-dimensional sublayer thickness, δ^+, is constant. We have determined the thickness of the viscous sublayer from 28 mean velocity profiles. When the thermistor data did not encompass enough of the logarithmic layer to determine the log layer shear accurately, we used (4) with $k = 0.4$ to extrapolate the velocity at the top of the heated thermistor profile downward to determine the sublayer thickness. To examine how well δ^+ agrees with universal similarity, we have plotted the dimensional sublayer thickness, δ, against ν/u_* (Fig. 4). Inspection of Figure 4 shows that δ does scale with ν/u_* but not perfectly. Rather than δ^+ being between 11 and 12 as in laboratory studies, it varies from 8 to 20 in our data.

DISCUSSION

The variability in δ^+ suggests some questions:

1. Does the scatter in Figure 4 reflect true variation in δ^+ or experimental error?
2. If the variations are real, are they caused by small-scale irregularities of the sea bed?
3. What is the effect of a variable non-dimensional sublayer thickness on the flow above?

Figure I-4. The thickness of the viscous sublayer plotted as a function of the ratio of the kinematic viscosity to the friction velocity. The straight line represents the expected relationship for a non-dimensional sublayer thickness equal to 11.1.

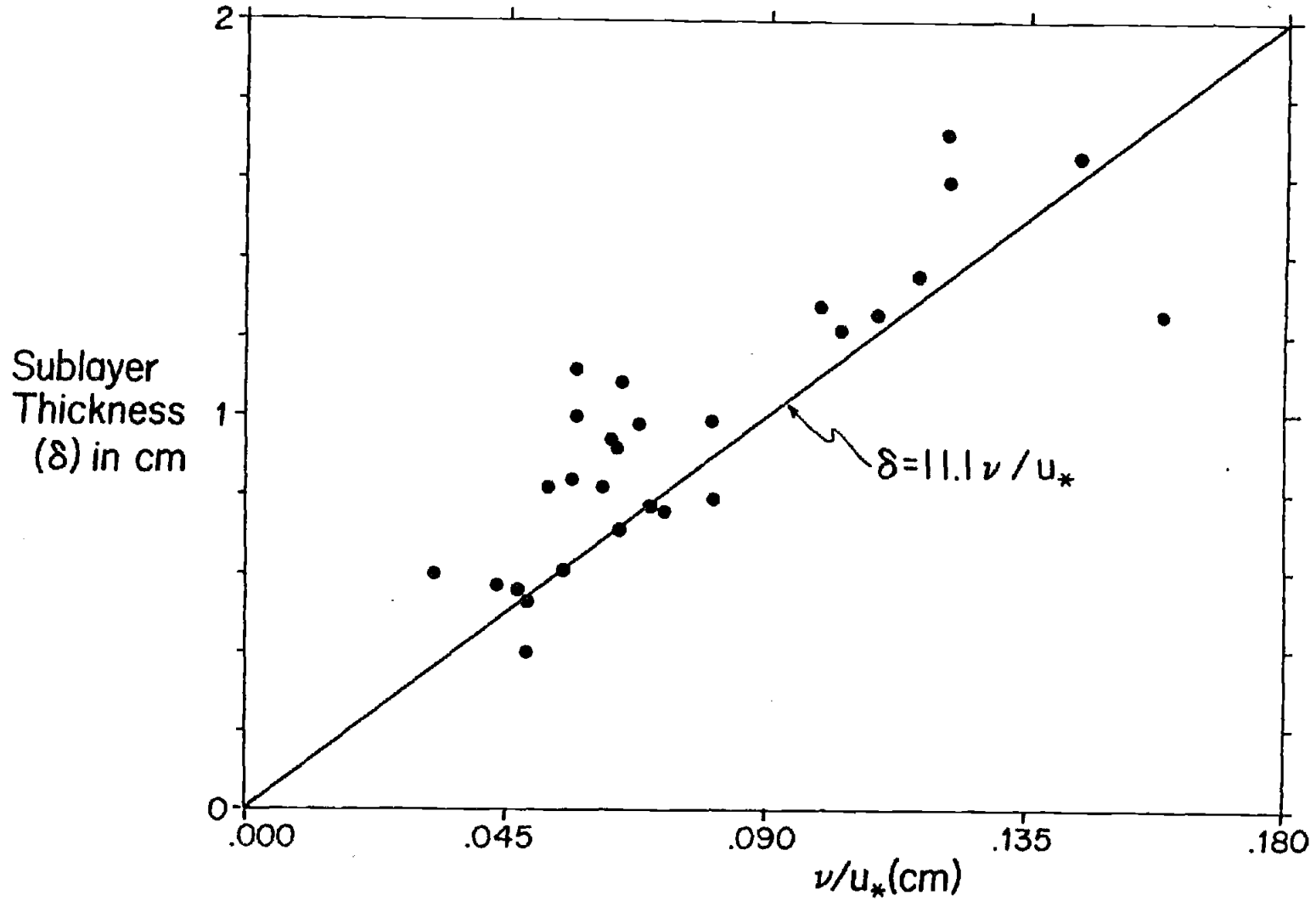
Sublayer
Thickness
(δ) in cm
2
1
0
.000
.045
.090
.135
.180
ν/u*(cm)
δ=11.1 ν / u*

Figure I-4.

We approach the first two questions by comparing mean velocities determined by the Savonius rotor 59 cm above the bed with the velocities at 59 cm which might be expected based on sublayer measurements alone. (Equation (8) indicates that δ and u_* completely specify the velocity at any position within the logarithmic layer above a smooth wall.)

We first evaluate the hypothesis that the variability in δ^+ is due to error in determining δ, the true value of δ^+ being 11.1. Using u_* for each time interval and the assumption that $\delta^+ = 11.1$, we have used (8) to calculate the expected mean velocity at 59 cm for each interval, taking $k = 0.4$. The calculated and measured velocities do not agree very well (Fig. 5). The agreement is markedly improved if the measured δ^+ values are used (Fig. 6). The observation that a variable δ^+ yields a better agreement than a constant δ^+ suggests that δ^+ is truly not constant and that the scatter in Figure 4 is not primarily due to experimental error.

The correlation (Fig. 6) between the currents determined by the rotor at 59 cm and those calculated by using the measured u_* and δ values in (8) has several important implications. The fact that the u_* and δ values used in (8) were derived entirely from heated thermistor data and yet the calculated velocities agree closely with the velocities from the rotor is evidence for the quality of the heated thermistor data. This agreement also indicates that form drag does not significantly influence the flow in the lowest 59 cm. The average difference between the rotor-derived velocities and those calculated from the heated thermistor data is only 0.47 cm/s, not much larger

Figure I-5. The relationship between the velocity at 59 cm determined by the Savonius rotor and that calculated from the friction velocity determined in the viscous sublayer and the assumption of a non-dimensional sublayer thickness equal to 11.1. The straight line indicates a 1:1 relationship between the measured and calculated velocities.

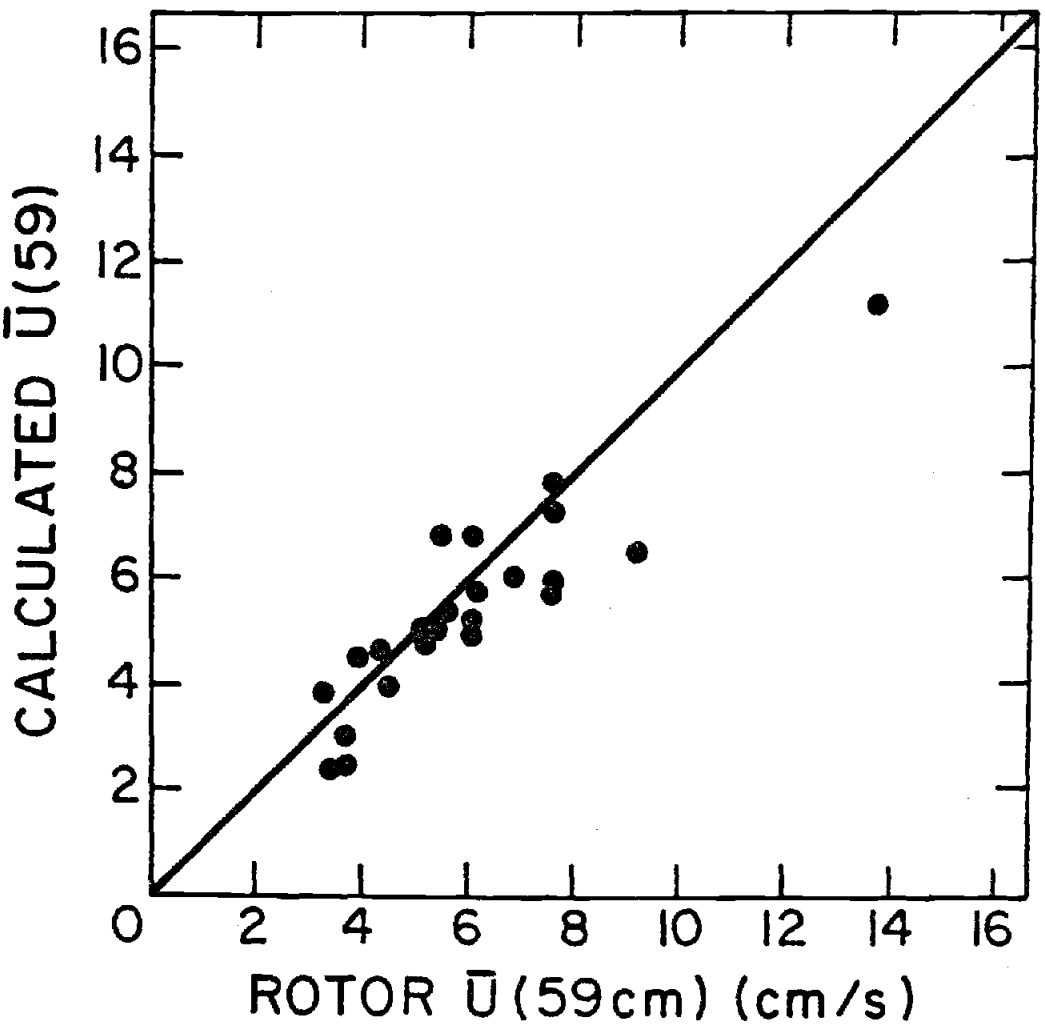

Figure I-5.

Figure I-6. The relationship between the velocity at 59 cm determined by the Savonius rotor and that calculated by using the measured values of the friction velocity and the sublayer thickness and equation (8). The straight line indicates a 1:1 relationship between the measured and calculated velocities.

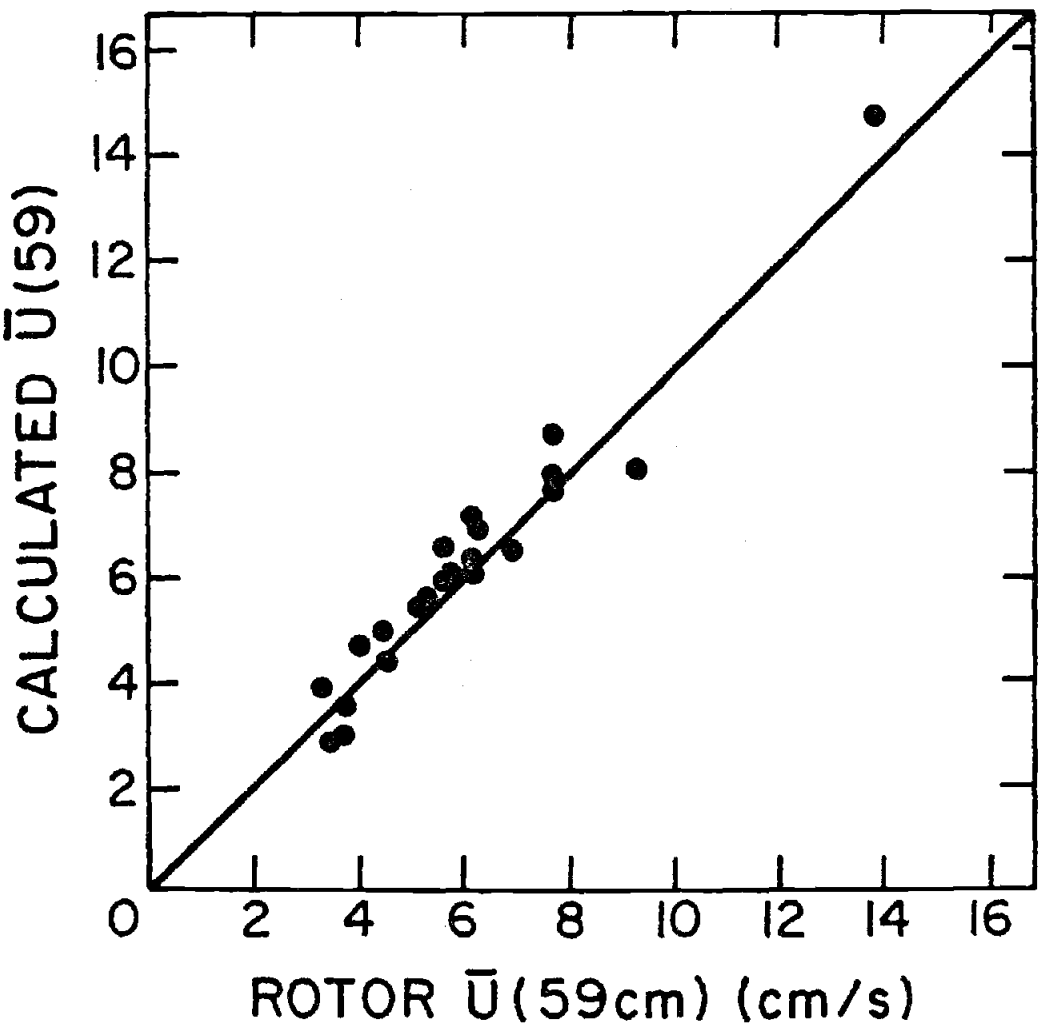

Figure I-6.

than the standard error of the rotor calibration (0.33 cm/s). Since the Savonius rotor was separated horizontally from the profiling thermistors by 1.3 m, it appears that, in general, the measured u_* and δ^+ values represent the average flow conditions over several square meters (or more) of the sea bed and do not merely reflect the local influence of small-scale irregularities.

To more rigorously test this hypothesis, we perform the following analysis: Assuming that currents measured by the Savonius rotor accurately represent the flow 59 cm above the bed, we use the u_* values from the sublayer data to calculate the δ^+ required (according to (8)) to predict the rotor velocity. If the deviations of the measured δ^+ values from a constant value were caused by experimental error or very small-scale irregularities, the "required" and measured δ^+ values should be uncorrelated. On the other hand, if the measured thicknesses represent the near-bed flow conditions over a horizontal scale of several meters, then there should be a significant correlation. A plot of the "required" and measured δ^+ values shows a definite relationship (Fig. 7). Testing the hypothesis that these values are uncorrelated is equivalent to testing the hypothesis that a regression line through the points in Figure 7 would have a slope of zero. Results of a statistical analysis using the t-test (Draper and Smith, 1966) indicate that this hypothesis can be rejected at the 99.9% confidence level. Therefore δ^+ is not constant at the ocean floor and most of the variability in δ^+ is not the result of small-scale irregularities but rather reflects flow variability extending over horizontal scales of several meters.

Figure I-7. The relationship between the measured non-dimensional sublayer thickness and the sublayer thickness "required" to perfectly predict the measured rotor velocity (at 59 cm) given the friction velocity determined from the sublayer measurements. The error bars shown indicate the change in the "required" non-dimensional sublayer thickness which would be caused by an error of 0.3 cm/s in the measured rotor velocity.

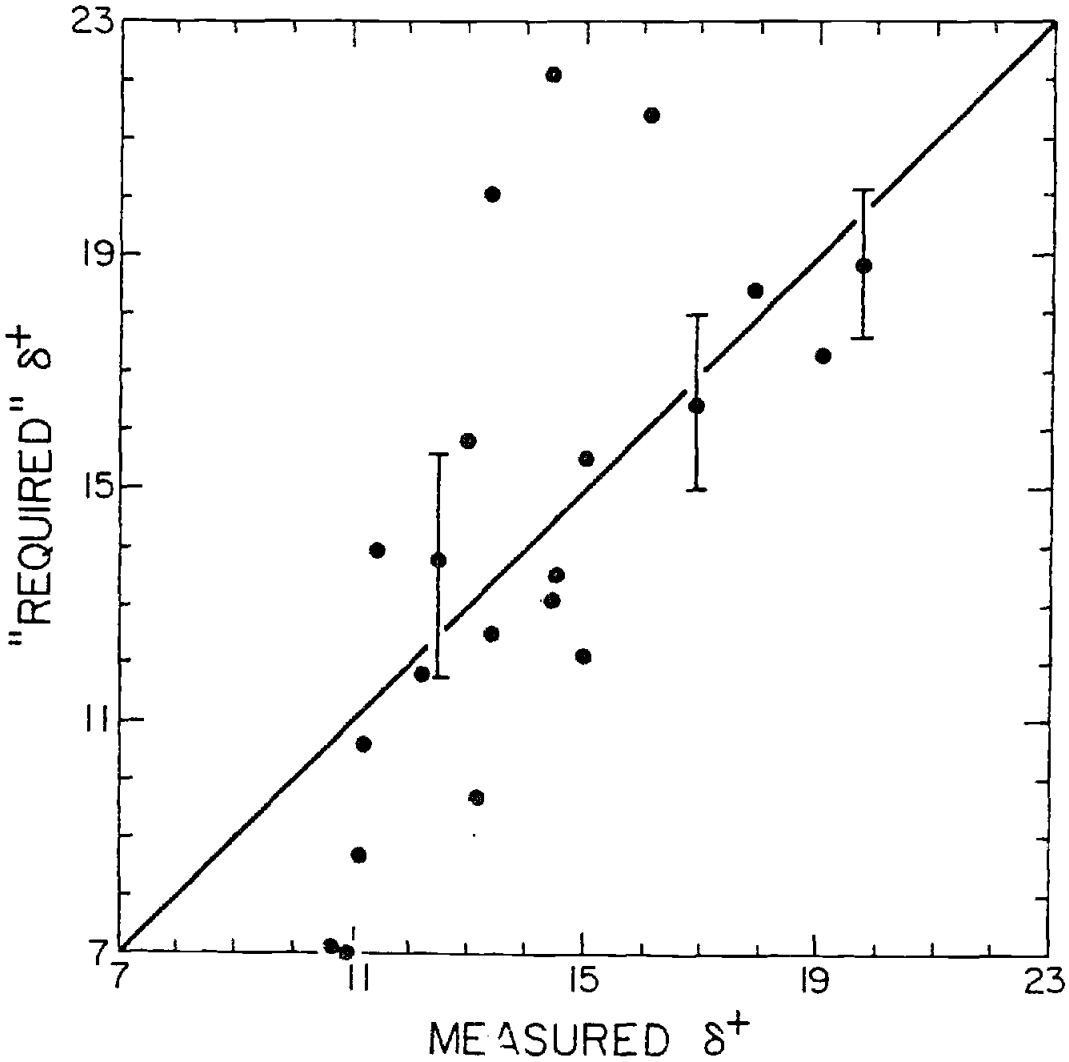

Figure I-7.

Are the deviations of our velocity profiles from the "universal velocity profile" (10) significantly greater than the deviations of typical laboratory data? Figure 8 is a standard non-dimensional plot of the data from all of our mean velocity profiles. The line $U^+ = z^+$ (for the linear velocity profile in the viscous sublayer) and the line $U^+ = 2.5 \ln z^+ + 5.1$ (for the "universal velocity profile" in the logarithmic layer) have been included for reference. We have also included the data from the rotor at 59 cm. The scaling implied by universal similarity fails to collapse our data to the "universal profile." Comparison with Figure 9 (reprinted from Monin and Yaglom, 1971) demonstrates that the deviations of our data from the "universal profile" are much larger than the deviations in the eleven laboratory investigations reported by Monin and Yaglom.

When a different symbol is used to identify each of the profiles upon which Figure 8 is based, it is obvious (Fig. 10) that the deviations from the "universal profile" are not due to measurement error but rather to variations in δ^+. The slope of the profiles (Fig. 10) is consistent, however, with $A \simeq 2.5$ (that is, with $k \sim 0.4$).

The effect of variations of δ^+ on the boundary layer flow follows from (8). For a given $\bar{U}(z)$ within the logarithmic layer, the friction velocity (and hence the stress at the bed) decreases as δ^+ increases. Thus computations of shear stress based on the velocity measurement from a single log layer sensor with the assumption that $\delta^+ = 11.1$ will overestimate the true stress if δ^+ is larger. This is also true for calculations of bed stress using (10) with $B = 5.1$. Our data indicates that differences between the true stress and that calculated

Figure I-8. Non-dimensional plot of all of the velocity data from this study. The straight line is for the so-called "universal velocity profile" in the logarithmic layer. The gap in the data represents the distance between the top of the heated thermistor profile and the rotor located at 59 cm above the sediment.

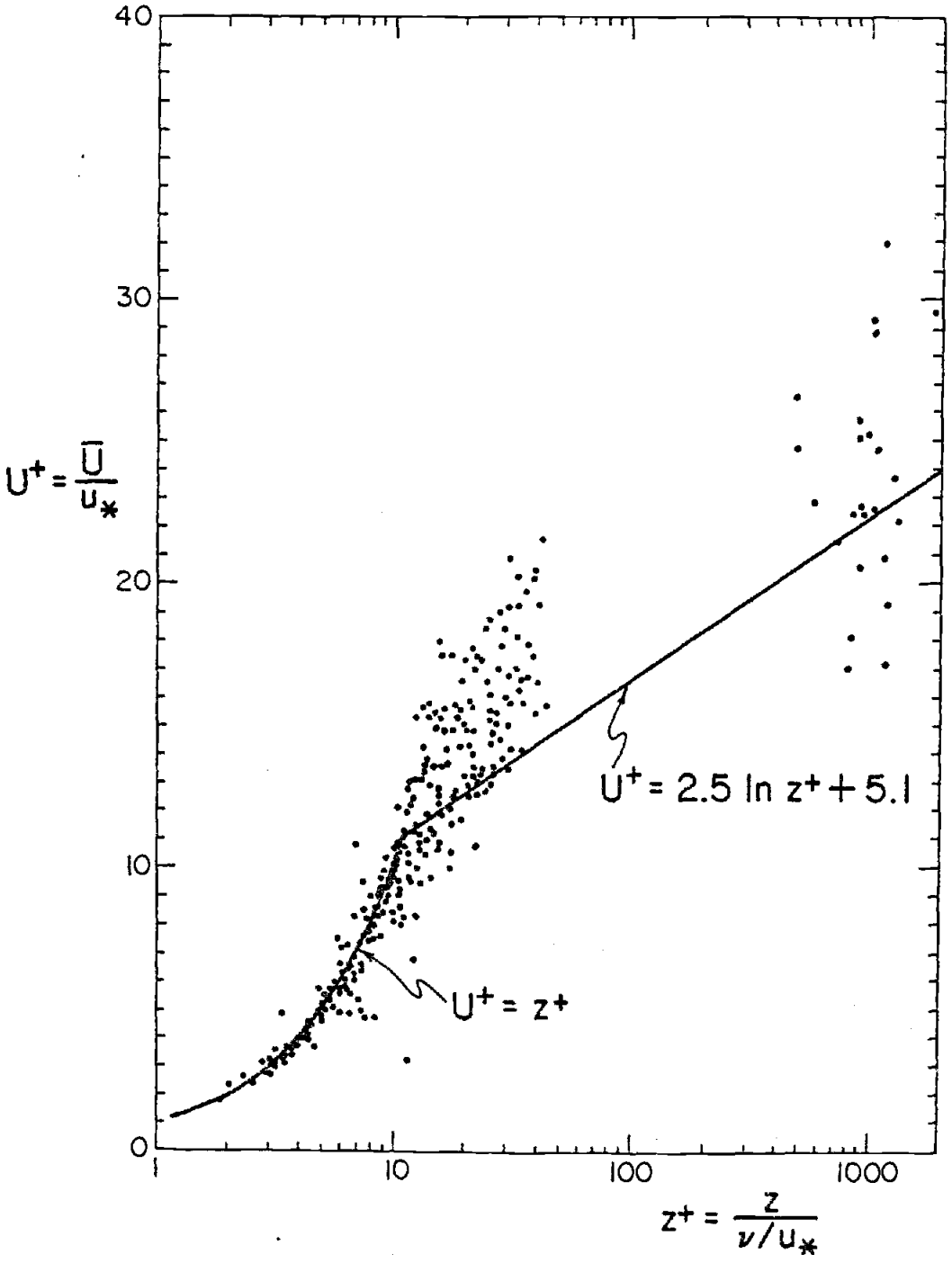

Figure I-8.

Figure I-9. Non-dimensional plot of the velocity data from 11 different laboratory investigations of turbulent boundary layers over smooth walls. (Reprinted from Monin and Yaglom, 1971.)

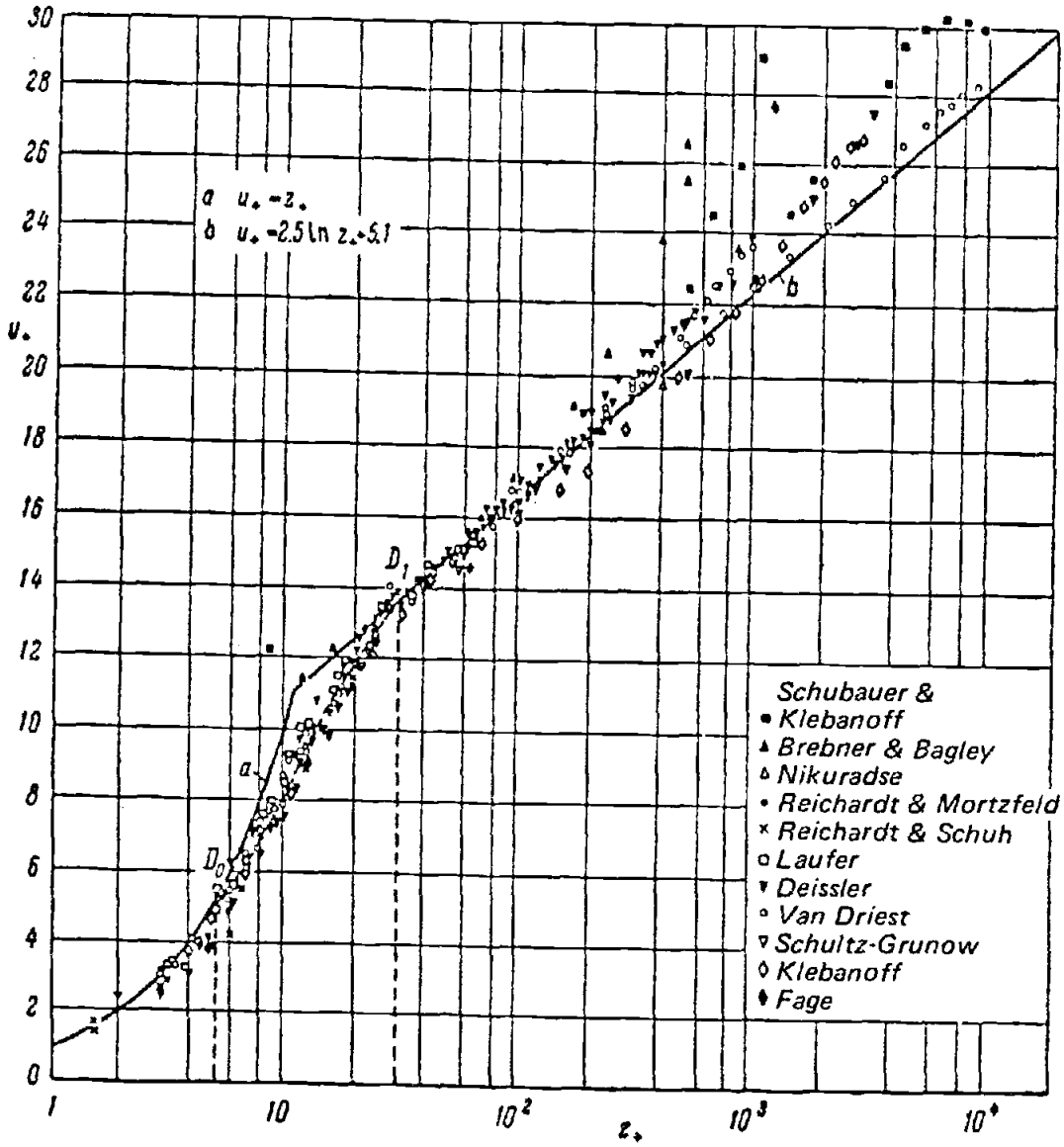
a $u_* = z_*$
b $u_* = 2.5 \ln z_* - 5.1$
u_*
z_*
D_0
D_1
Schubauer &
Klebanoff
Brebner & Bagley
Nikuradse
Reichardt & Mortzfeld
Reichardt & Schuh
Laufer
Deissler
Van Driest
Schultz-Grunow
Klebanoff
Fage

Figure I-9.

Figure I-10. Non-dimensional plot of the velocity data for three different time intervals in our experiment. The dashed line represents the velocity profile expected for a non-dimensional sublayer thickness of 11.1. The slope of both straight lines is that expected for von Karman's constant equal to 0.4.

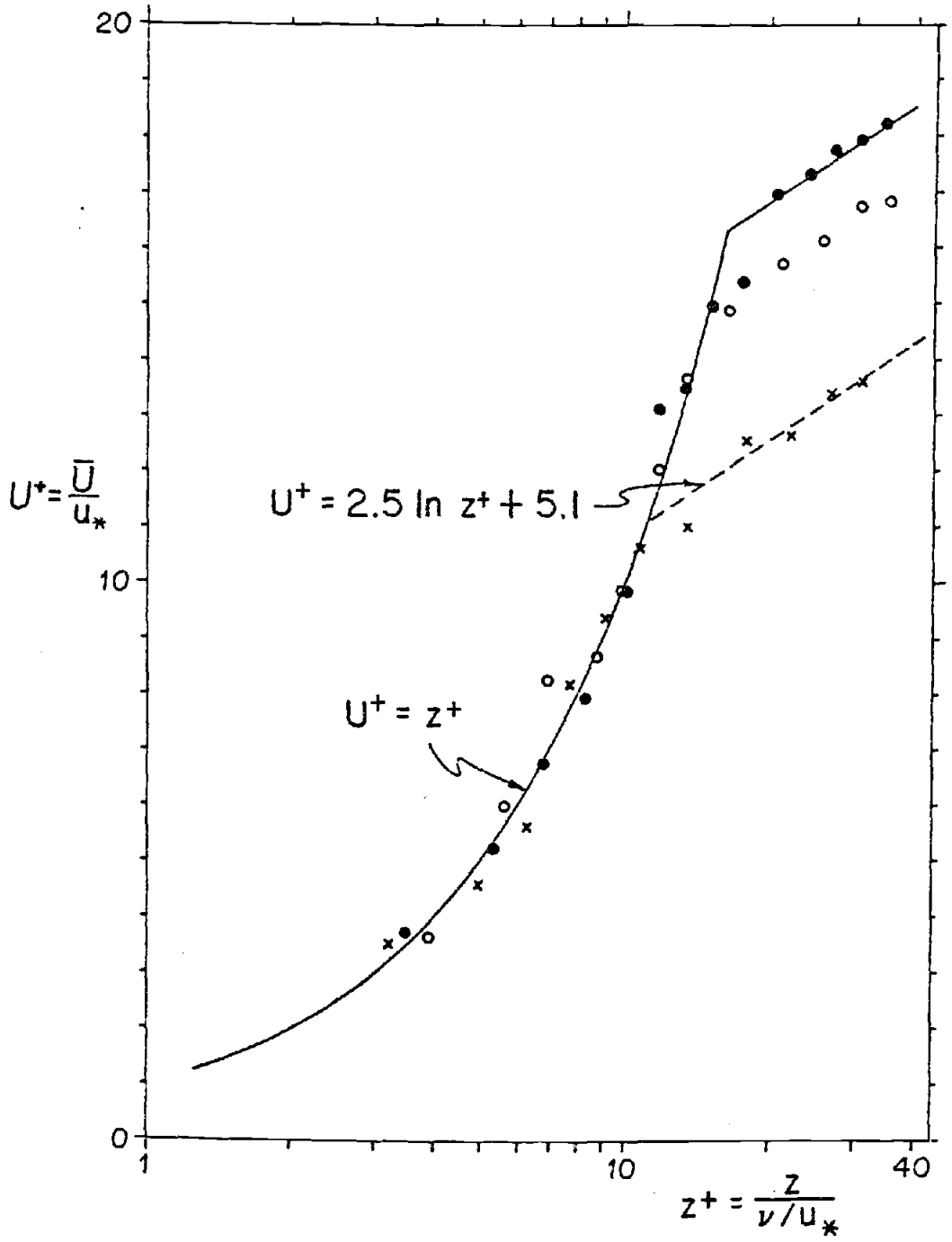

Figure 1-10.

from the rotor velocity assuming B = 5.1 ($\delta^+ = 11.1$) may be as large as 60% of the true stress.

While our experiments are, to our knowledge, the only studies in which velocity measurements have been made within the viscous sublayer of a geophysical flow, data from several other geophysical boundary layer experiments also suggest that the concept of universal similarity of smooth-wall boundary layer flows may not always be applicable. Csanady (1974) summarized the results of experiments by Portman (1960) and Sheppard et al. (1972) in which determinations of z_o from wind velocity profiles over lakes indicated that z_o was significantly less than expected for a universally similar, neutrally-buoyant flow. Equating $\bar{U}(z) = (u_*/k) \ln (z/z_o)$ with (8), it is clear that for hydrodynamically smooth flow, the so-called "roughness" length z_o is simply a function of the thickness of the viscous sublayer:

$$z_o = \delta \exp(-\delta u_* k/\nu) \tag{13}$$

and that the commonly used expression

$$z_o = \nu/9u_* \tag{14}$$

is appropriate only for the special case in which $\delta^+ = 11.6$. Because the Portman (1960) and Sheppard et al. (1972) data indicated that z_o was often smaller than expected from (14), Csanady concluded that δ^+ was sometimes larger than 11.6. Not only was δ^+ not 11.6 in these experiments, but it varied inversely with u_* at low wind velocities, ranging from less than 11 to 40.

What causes the variability in δ^+?

Energy balance considerations led Csanady (1974, 1978) to conclude that sublayer thickening is likely to result from any process which extracts energy (for example as work against buoyancy forces) from the region of the viscous sublayer. Csanady (1974) concluded that the sublayer thickening over lake surfaces during light winds may have been the result of work against surface tension. He proposed that energy was extracted due to the horizontal variation in surface tension caused by organic films and other impurities at the air-water interface. Arya (1975b) found an increase in δ^+ with increasing stability in thermally stratified flow over a flat plate and attributed it to work against buoyancy forces. For very unstable stratification, the sublayer was thinner than expected for a universally similar neutrally-buoyant flow. Arya's results suggest that the lack of agreement of our data with universal similarity could be related to stability effects.

Gust (1976) reports laboratory experiments in which the thickness of the viscous sublayer for dilute seawater-clay suspensions was two to five times larger than for comparable suspension-free flows. Gust suggested that this thickening was related to elastic deformation of clay mineral aggregates by the turbulent flow. Gust's data suggests that the value of u_* determined from the slope of the profile in the logarithmic region of the flow was significantly larger than the value determined from the shear in the sublayer. This relationship is not observed in our data.

We have attempted to correlate our δ^+ measurements with some other quantities. Data from the 25 cm path-length beam transmissometer (optical axis located 21 cm above the sediment), and from a similar unit mounted on a freely-falling microstructure profiler (Newberger and Caldwell, 1981) indicate low suspended sediment concentrations (0.4 to 3 mg/liter), much less than the smallest concentration (150 mg/liter) in Gust's experiments. This optical data shows no correlation with δ^+. It is possible, however, that significant concentration gradients existed between the bed and the lowest positions of the optical sensors.

Temperature profiles from the microstructure profiler demonstrate that the bottom few meters were within a few millidegrees of being isothermal. Salinity profiles were not obtained, but previous experience (Caldwell, 1978) suggests that salinity variations within the bottom layer are smaller than 0.002 parts per thousand (below the resolution of the best instrumentation). Thus we lack the information required to infer any influence of density gradients on δ^+.

Because Gordon (1975) suggests that drag coefficients and some turbulence parameters may vary with acceleration in tidal flows, we looked for correlations of δ^+ with tidal phase. Because a strong tidal signal was not apparent in the velocity, the tidal phase was determined from bottom pressure measurements. No correlation was found. We have also analyzed velocity profiles from a number of short intervals in which the flow was either accelerating or decelerating ($|dU/dt| < 0.012$ cm s^{-2}), but have found no significant relationship between δ^+ and the magnitude or sign of the acceleration.

We find no correlation between δ^+ and u_*. A series of velocity profiles taken over several hours in which the flow direction was nearly constant shows variability in δ^+ from 11 to 20, again suggesting that differences in bottom topography are not the cause of the variations of δ^+.

We conclude that our data are not adequate to determine what processes cause the variability in δ^+. To resolve this question, vertical profiles of density at the platform site may be required, and such profiles must include the effect of suspended particles, particularly in the sublayer.

How representative are these observations?

It should be emphasized that the data which form the basis of this paper were obtained from one experiment conducted at several water depths on the Oregon shelf during June 1979 and can only be assumed to represent the flow conditions during this experiment. While this data is consistent with the assumption of a constant stress layer extending from the sediment-water interface up to 59 cm above the sediment, data from an experiment conducted at 199 m water depth in October 1978 (Chriss and Caldwell, 1981a) demonstrate that the constant stress assumption was valid only up to 11 to 15 cm above the bed. The shape of the velocity profiles from this October 1978 experiment suggest that form drag significantly influenced the flow farther than 11 to 15 cm from the bed. Stress calculated from the slope of the logarithmic profile in this region was several times

larger than the true bed stress (determined from the shear in the viscous sublayer). Thus while both experiments demonstrated the existence of a viscous sublayer just above the sediment-water interface, the boundary layer flow during the October 1978 experiment appears to have been significantly influenced by form drag whereas the flow measurements reported in this paper suggest no such influence during the June 1979 experiment.

The extent to which these results are typical of flow conditions on the shelf will only be determined after additional experiments are performed in a wider variety of locations.

CONCLUSIONS

Data obtained during this experiment indicate that the boundary layer flow at the ocean floor was hydrodynamically smooth, and has been used to test the assumption that the flow behaved as a universally similar, neutrally-buoyant flow over a smooth wall. Data analysis indicates that:

1. Von Karman's constant at the ocean floor is not significantly different from the value determined in the laboratory and in other geophysical flows.
2. The non-dimensional thickness of the viscous sublayer at the ocean floor is not constant. Thus the boundary layer flow cannot always be described by the equations for a universally similar, neutrally-buoyant boundary layer over a smooth wall.

3. Bed stress estimates obtained from the conventional equations for such flows may not always yield accurate results.
4. The non-dimensional sublayer thicknesses are representative of flow conditions averaged over several square meters of the sea floor, and deviations of the non-dimensional thickness from a constant value are not the result of measurement error or small-scale bed irregularities.
5. In contrast with an earlier experiment (Chriss and Caldwell, 1981a), flow measurements in this experiment are consistent with the assumption of a constant stress boundary layer extending to at least 59 cm above the sediment.

CHAPTER II

EVIDENCE FOR THE INFLUENCE OF FORM DRAG ON BOTTOM BOUNDARY LAYER FLOW

T. M. Chriss

School of Oceanography

Oregon State University

Corvallis, Oregon 97331

Submitted to Journal of Geophysical Research

ABSTRACT

An experiment in 199 m water on the Oregon shelf has produced the first set of field data yielding continuous current speed profiles down to the sediment-water interface. These profiles show that the velocity structure above the viscous sublayer is consistent with that expected when form drag influences the boundary layer flow. They show two logarithmic profile regions, each yielding a different bed stress estimate. The stress calculated from the upper one reflects the influence of form drag and is more than four times the bed stress determined from the shear in the viscous sublayer. When form drag is significant, the application of logarithmic profile or Reynolds stress techniques to measurements more than a few tens of centimeters from the bed may yield bed stress estimates inappropriate for use in sediment transport or entrainment calculations. Large roughness length or drag coefficient values cannot be taken as evidence that a viscous sublayer does not exist.

INTRODUCTION

Smith (1977) emphasizes that, for the study of sediment transport on continental shelves, it is important to distinguish between the contribution of skin friction and that of form drag to the total boundary stress. Skin friction here refers to the shear stress averaged over a few tens of grain diameters, whereas form drag is that portion of the total stress caused by the irregularity of the boundary. Although flow in the upper part of the boundary layer is influenced by the total stress, erosion and near-bed sediment transport are related to skin friction alone. When form drag is significant, the simple logarithmic profile expected in turbulent flow over a horizontally homogeneous surface may not be found. Instead, the profile may consist of several regions with different logarithmic slopes (Arya, 1975a). In the outer region the mean flow is expected to obey the usual logarithmic law,

$$\bar{U}(z) = (U_*/k)\ \ln(z/Z_o) \qquad (1)$$

where k is von Karman's constant, Z_o is a large-scale roughness parameter reflecting the influence of both small-scale topography and skin friction, and $U_* = (\tau_t/\rho)^{1/2}$ is a friction velocity based on the total stress, τ_t. Closer to the boundary, an internal boundary layer may develop in which the mean profile is also logarithmic

$$\bar{U}(z) = (u_*/k)\ \ln(z/z_o) \qquad (2)$$

but where the friction velocity, u_*, and the roughness parameter, z_o, now reflect the conditions of the surface between the large-scale roughness elements. This friction velocity, u_*, is based on the

local skin friction (which may be spatially variable) rather than on total stress. (If the intervening surface is hydrodynamically smooth, z_o is not determined by the small-scale roughness characteristics, but rather by the thickness of the viscous sublayer [Chriss and Caldwell, 1981b].) Although this description suggests a profile composed of two intersecting segments, Smith (1977) and Smith and McLean (1977) demonstrate that multiple roughness scales can generate velocity profiles with more than two. Thus when form drag is important the constant-stress assumption will not be valid.

In an earlier paper (Caldwell and Chriss, 1979), we demonstrated the existence of the viscous sublayer in the bottom boundary layer and found a logarithmic layer above it. In examining additional data from the experiment, segmented profiles in the logarithmic region were found (Figures 1 and 2), as expected if form drag influences the flow. When the original data set was re-analyzed, using thinner averaging intervals in the upper portion of the profile and also incorporating both upward and downward traverses, it too shows two distinct logarithmic slopes. (In the original study, only downward traverses were used.) Although deviation from a single logarithmic form is not always large, the slope of the logarithmic regression is significantly different in the two regions, implying that the turbulent stress above is significantly larger than it is nearer the bed.

This experiment represents the first time in a natural environment that continuous profiles of current velocity have been obtained down to the sediment-water interface, and thus provides an ideal, though somewhat limited, data set with which to evaluate the influence

Figure II-1. Typical mean velocity profile for the October 1978 experiment. The distance from the sediment has been plotted using a logarithmic scale. The dashed line near the sediment represents a linear fit to the data in the viscous sublayer. The solid lines represent fits to the data in the lower and upper logarithmic regions of the velocity profile. The region between the dashed line and the lower solid line is the so-called "buffer" region where the velocity profile obeys neither a linear nor a logarithmic law. (Data interval number 4 of Table 1).

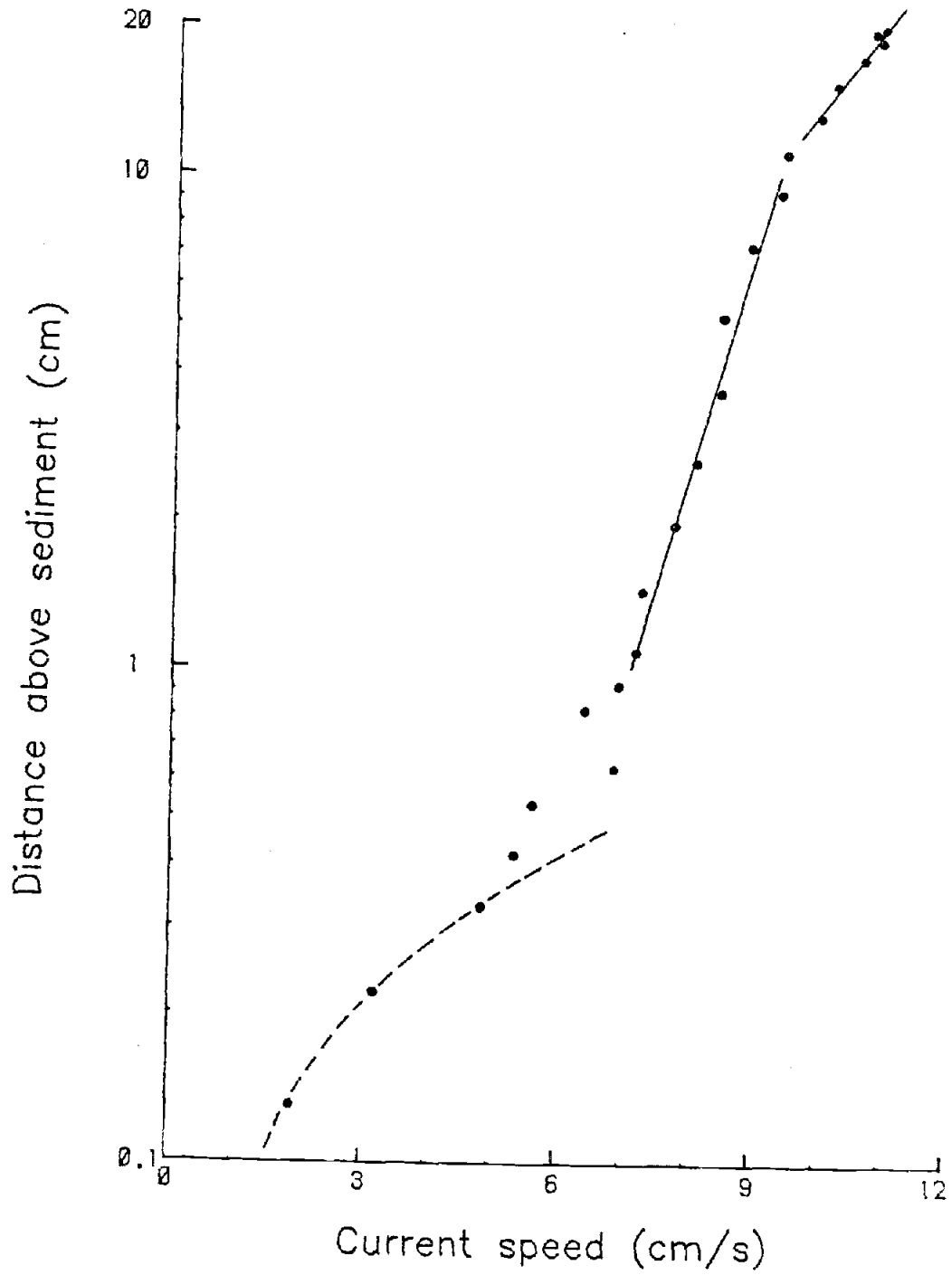
20
10
1
0.1
Distance above sediment (cm)
0
3
6
9
12
Current speed (cm/s)

Figure II-1.

Figure II-2. Same data as Figure II-1, but plotted with a scale which emphasizes the logarithmic regions of the velocity profile.

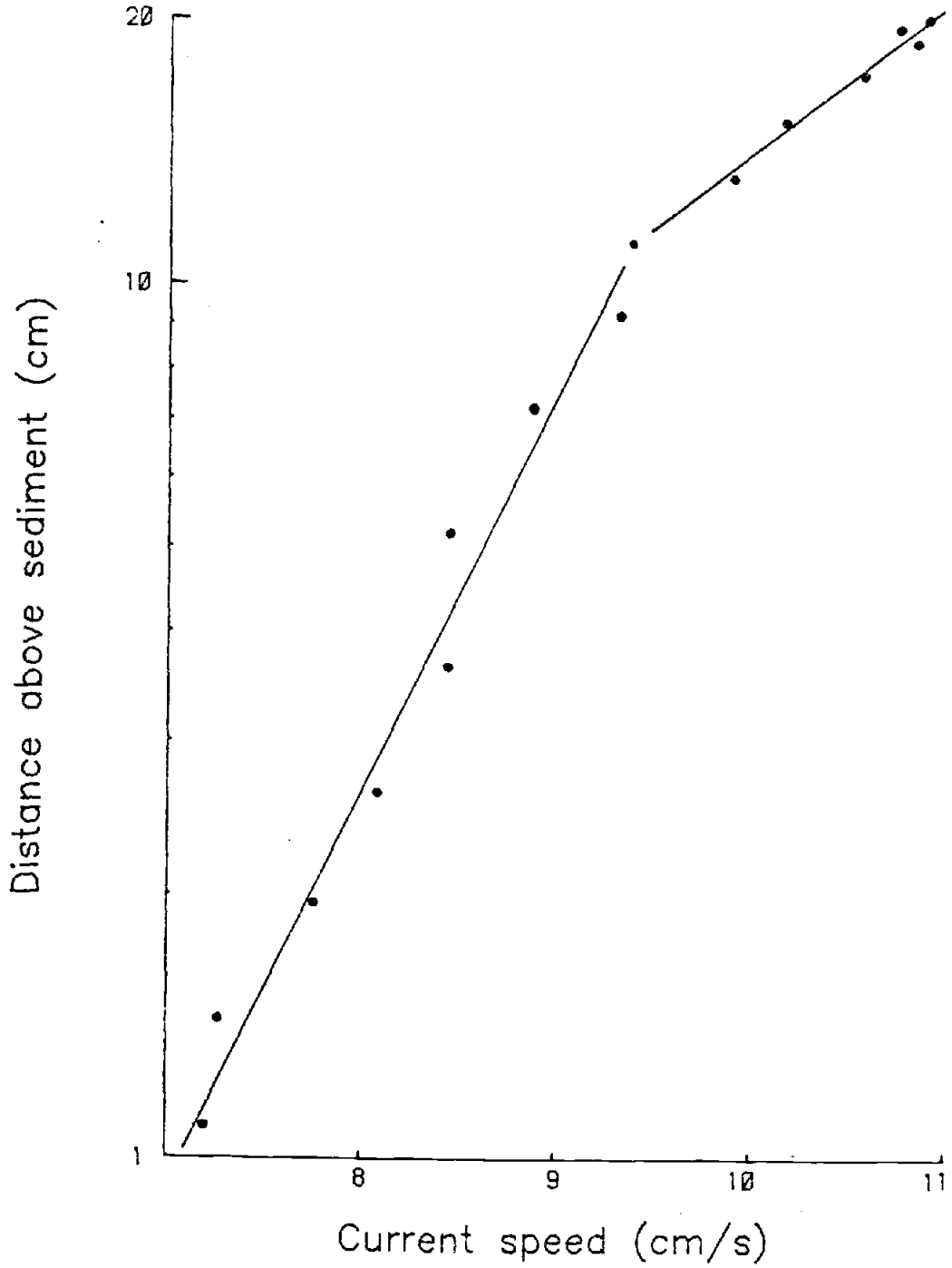

Figure II-2.

of form drag on boundary layer flow and on sediment transport calculations. Estimates of bed shear stress using sensors located further than 15 cm from the bed were significantly influenced by the presence of form drag, and entrainment calculations using such estimates would have been based on stresses more than four times the true stress at the bed.

THE EXPERIMENT

The experiment was carried out on October 11 and 12, 1978 at 45°20'N (199 m total water depth) on the Oregon shelf. The surface sediment was silty sand (Runge, 1966). Profiling heated-thermistor velocity sensors were mounted on a 2 m high tripod placed on the sea floor. Most data come from an 18-hour deployment. Some additional data were obtained in a 4-hour deployment. A data acquisition system on the tripod sampled each thermistor every 1.5 seconds during the 18-hour deployment and every 0.38 seconds during the 4-hour deployment. Additional instrumentation included profiling and stationary temperature sensors, stationary heated-thermistor sensors, Savonius rotors, a 25 cm path-length beam transmissometer, a high-resolution pressure transducer, and a time-lapse motion picture camera which monitored the condition of the sensors.

Current was supplied to each heated thermistor to heat it approximately 20°C above the water temperature. Because the velocity calibration is a function of both the water temperature and the orientation of the flow with respect to the thermistor, each thermistor was post-calibrated at the temperatures and flow directions

observed during the experiment. Calibrations were performed by towing in a 1 m radius annular channel, fitting to the formula

$$P/\Delta T = A + BU^N \qquad (3)$$

where P is the power dissipated in the thermistor, ΔT is its temperature rise, U is the speed, and A, B, and N are experimentally determined. Inversion of this formula allows the calculation of speed from measurements of $P/\Delta T$, which is computed from the output of a bridge circuit. Using (3) with empirically-determined A, B, and N, speed can be determined within 0.1 cm/s in the laboratory. The heated thermistors measure speed only, flow direction is determined by a small vane.

The heated thermistors were carried up and down by a crank-and-piston mechanism driven by an underwater motor. The mechanism was mounted outside one tripod leg, to provide unobstructed flow through an arc of 300 degrees. Only for times when the flow was completely unobstructed were data analyzed. The profiling period was one minute. The vertical travel was 21 cm. During the 4-hour deployment, the thermistors came within a few cm of the sediment-water interface, but during the 18-hour deployment the thermistors penetrated the sediment 0.3 cm. The vertical position of the sensors was determined by a potentiometer connected to the motor shaft. Calibration with a dial indicator showed that the vertical position was known within 0.03 cm. The location of the sediment-water interface was taken to be the zero-velocity intercept of the linear velocity profile within the viscous sublayer. Although the thermistors did not always penetrate

the sublayer during the 4-hour deployment, they did penetrate it during one interval of very low current, allowing the interface position to be determined.

DATA ANALYSIS

Mean profiles were constructed by averaging over time intervals 28 to 44 minutes long, each interval containing many traverses. Intervals were chosen for steadiness of speed and direction. Within 1.2 cm of the sediment the traverse was divided into layers 0.1 cm thick for averaging; above 1.2 cm, the averaging layers were 1 to 2 cm thick. The mean for each layer was determined by averaging all measurements within it during the repeated traverses. Before averaging, the effect of the profiler's vertical velocity was removed by vector subtraction from the measured velocity. Corrections for sampling error due to variability of the large-scale flow were made using measurements from a stationary sensor 20 cm above the sediment (Badgley et al., 1972).

The shear in the viscous sublayer was determined by linear regression, and bed stress was computed using the relationship

$$\tau_b = \rho\nu \, \partial\bar{U}/\partial z \qquad (4)$$

where ρ and ν are the density and kinematic viscosity of sea water. Logarithmic regression in the lower segment of the logarithmic region yielded estimates of z_o and k, assuming equality of the sublayer stress with that in the lower logarithmic layer. It should be emphasized that in hydrodynamically smooth flow, z_o reflects only the

sublayer thickness and is not determined by the grain size of the sediment (Chriss and Caldwell, 1981b).

Logarithmic regression in the upper segment yielded estimates of Z_o and U_* (Table 1). For the latter calculation, k in the upper segment was taken to be 0.4. A second sensor produced qualitatively similar segmented profiles. Detailed analysis of this data was discontinued, however, because large and variable k estimates (0.8 to 1.6), occasional negative shears, and evidence of intermittent sensor malfunction indicate that this data may not be quantitatively reliable.

Before considering the significance of the segmentation of the profiles, we consider two questions: (1) Are these profiles representative of this region, or do they merely reflect some unusual conditions in the immediate area of the tripod and (2) Is the segmentation an artifact of our measuring system? The question of representativeness can be approached by considering that although all of the data of Table 1 and Figures 1 and 2 came from the 18-hour deployment, similar segmented profiles were obtained during the 4-hour deployment. Because of the small chance of setting the tripod down in the same spot twice, these results must be representative to some extent. To answer the second question, we consider profiles obtained at the beginning of each deployment. As the tripod was lowered to the sea floor, the profiler mechanism was operating but in a retracted position to prevent damage to the sensors. A timed release lowered the mechanism to the sediment 20 to 40 minutes later. So at the beginning of each deployment the sensors were being traversed between 26 and 47 cm above the sediment. These profiles show no segmentation,

Table 1. Friction velocities, roughness lengths and von Karman's constants for individual data intervals.

Data Interval	Flow Direction†	u_* (sublayer) (cm/s)	k (for lower log region)	z_o (cm)	Z_o (cm)	U_* (upper log region) (cm/s)
1	90	.27	.40 $\pm$ .04	2.5×10^{-3}	.29	.62
2	90	.30	.88 $\pm$ .24	3.8×10^{-4}	1.39	.62
3	270	.51	.41 $\pm$ .05	6.2×10^{-4}	.080	1.00
4	270	.47	.49 $\pm$ .03	6.6×10^{-4}	.27	1.02
5	110	.19	.53 $\pm$ .10	2.5×10^{-4}	1.23	.62

†Flow direction is given with respect to tripod coordinate system.

evidence that the profiler mechanism itself does not cause it.

Although wave orbital velocities to 3.5 cm s^{-1} were obvious during the 18-hour deployment (Caldwell and Chriss, 1979), in the 4-hour deployment no oscillatory motion was observed. Segmented profiles were found in both deployments, so the segmentation is not caused by surface waves.

DISCUSSION

Although the shape of the profiles suggests that form drag was significant, we have no direct information about bedforms or other small-scale features in the area. We tried to obtain stereo photographs with a borrowed camera system, but were foiled by a faulty triggering mechanism. The time-lapse camera on the tripod did obtain low quality photographs of the bed, but, because the field of view was restricted to one square meter, and because the lighting was optimized for sensor observation, the absence of obvious features in these photographs is not conclusive. Features just outside the field of view could have significant influence on the flow. Because the photographic information is inconclusive, estimates of the size and spacing of roughness elements must come from analysis of the velocity profiles themselves. In a later section of this paper, we will, however, present some photographic evidence from an area 65 km to the south.

The following analysis is restricted to the 18-hour deployment because during the shorter deployment the currents were extremely small so the observations are less accurate.

Estimates of Roughness Element Geometry

Elliot (1958) derives the following expression for the growth of an internal boundary layer following a change in roughness:

$$(\delta_{IBL}/z_o) = a(x/z_o)^{0.8} \qquad (8)$$

where δ_{IBL} is the thickness of the internal layer a distance x from a change in the surface roughness, z_o is the roughness length for the internal layer, and 'a' depends on the ratio of z_o to the roughness length, Z_o, for the flow outside the internal layer:

$$a = 0.75 - 0.03 \ln(z_o/Z_o) \qquad (9)$$

As noted by Arya (1975a), Elliot's model is supported by measurements over a hot runway (Elliot, 1958), and also by the observations of Bradley (1968) under near-neutral conditions, and by the results of a second-order closure model by Rao et al. (1974).

Arya (1975a) suggests that Elliot's model may also apply to the growth of an internal boundary layer in the region between large-scale roughness elements and, like Smith (1977) and Smith and McLean (1977), uses Elliot's results to model the influence of form drag on velocity profiles. The position, z_*, of the kink in the profiles is assumed to represent the local thickness (δ_{IBL}) of the developing internal boundary layer. Applying the model, we estimate x from determinations of z_o, Z_o and z_* from our profiles. These estimates (Table 2) suggest that elements capable of explaining our velocity profiles would not have been within our camera's field of view. It is unlikely that oscillatory ripple marks (Komar et al., 1972) are responsible, because the maximum ripple spacing reported by Komar et

Table 2. Estimated distances from sensor to roughness elements. Calculated using measured z_*, z_o, and Z_o values and the theory of Elliot (1958).

Data Interval	Flow Direction	z_* (cm)	x (cm)
1	90	11.3	107
2	90	14.3	200
3	270	10.8	142
4	270	10.9	135
5	110	14.3	220

al. was only 21 cm, 5 to 10 times smaller than our estimates. Miller and Komar (1980) suggest that the maximum ripple length is a function of grain size. Using their results and the grain size in our area, we calculate that the maximum ripple spacing would have been less than 10 cm.

Height estimates for the elements can be obtained from a model developed by Arya (1975a) for estimation of Z_o and τ_t over Arctic pack ice. Because we lack the detailed topographic information required to verify the assumptions of the model, we will apply the model formally but interpret the results of our analysis with some caution. Arya finds:

$$\ln(Z_o/z_o) = 4/5[\ln(h/z_o) + \ln(1/\lambda - b/h - B/h)]$$
$$\cdot [1 - (k_u/k_L)\{1 - m\lambda + (C_D\lambda/2k_L^2)(\ln h/z_o)^2\}^{-1/2}] \qquad (10)$$

Here h is the height of the elements, λ is the ratio of h to their spacing, s, b is their width, and B is the sum of the widths of the regions of separated flow which may exist around the roughness elements. Over streamlined elements, the flow may not separate and B may be neglected. C_D is a drag coefficient which relates the form drag on the element to the mean velocity (at z = h) of the upstream flow:

$$F_D = \frac{1}{2} C_D \lambda \rho \bar{U}(h)^2 \qquad (11)$$

Here F_D is the form drag per unit area of the bed and ρ is the density of the fluid. The constant m in (10) is taken by Arya to be 20. Equation (10) differs from equation 15 of Arya in not assuming equal-

ity of the values of von Karman's "constants" (k_L and k_u) inside and outside the internal boundary layer. We will use (10) because, although our estimates of k are not always 0.4 in the internal layer (Table 1), we have no evidence that k is not 0.4 above. Although deviations of k_L from the commonly accepted value of 0.4 may simply reflect uncorrected sampling or measurement errors in our data, some laboratory data suggests that k_L is not always 0.4 in internal boundary layers between roughness elements (Paola et al., 1980). Use of (10) allows us to use measured values of k_L while still using 0.4 outside the internal boundary layer.

Although (10) was derived to predict Z_o, it can be solved (iteratively) for h, using measured values of Z_o, z_o and k_L from our profiles, together with estimates of the other quantities. We set b to 70 cm; changing it by 50 cm changes h by only 10%. We set B to zero, but with our data the model is not very sensitive to the value of B. The spacing s was taken to be 348 cm based on estimates of x (Table 2) for flow directions 180° apart. Because of the lack of information about element shape, the choice of C_D is not obvious, so we have used a range of values from the literature (Arya, 1973; Smith and McLean, 1977).

The results of these calculations (Table 3) yield plausible element heights for the larger drag coefficients. (We have excluded heights calculated for the smaller drag coefficients for some of the intervals because these calculated heights violate an assumption of the model which is that λ is less than 1/m.) We conclude that if the model is applicable, flow over roughness elements 4 to 17 cm high

Table 3. Roughness element heights (cm) estimated by applying the model of Arya (1975) and various assumptions about the roughness element drag coefficient (C_D).

Data Interval	Assuming $C_D = 1.00$	Assuming $C_D = .84$	Assuming $C_D = .4$
1	6.4	7.5	14.9
2	16.7	†	†
3	3.9	4.7	9.1
4	6.3	7.4	15.2
5	16.0	†	†

†Calculated heights have been omitted because they violate the assumptions of Arya's model.

with drag coefficients of 0.8 or larger could generate our velocity profiles.

Photographic Evidence from the Oregon Shelf

As mentioned earlier, we have no photographic information about small-scale bottom topography in the area of the study. We do, however, have some information from a large number of bottom photographs obtained 65 km to the south, from an area of the same water depth (200 m) and similar sediment texture. These photographs, furnished by Andrew Carey of Oregon State University, were obtained as part of a study of the sampling efficiency of beam trawls. A single camera was mounted just ahead of the trawl for the purpose of photographing the sediment prior to sampling. Although current generated bedforms are absent, typical bottom photographs (Figures 3 and 4) reveal two dominant types of biologically related roughness elements. The sea urchins (typically 6-8 cm in diameter) are ubiquitous, although their abundance varies significantly. The "mounds" represent sediment expelled from burrows which were possibly occupied by polychaete worms. By comparison with the known size of the urchins, the height of the mounds can be estimated to vary from less than a few cm to more than 15 cm. The spacing of the mounds varies greatly from photograph to photograph as well as within a single photograph. In some cases mounds nearly coalesce and form ridges. Photographs from different years all show features similar to those in Figures 3 and 4. Because the density and height of the roughness elements vary from photograph to photograph, and because stereo photos are not

Figure II-3. Bottom photograph representative of those obtained from 65 km south of our area of study, in a region of the same water depth (200 m) and similar sediment texture. See text for description.

Figure II-3

Figure II-4. Additional photograph from the area described in Figure II-3.

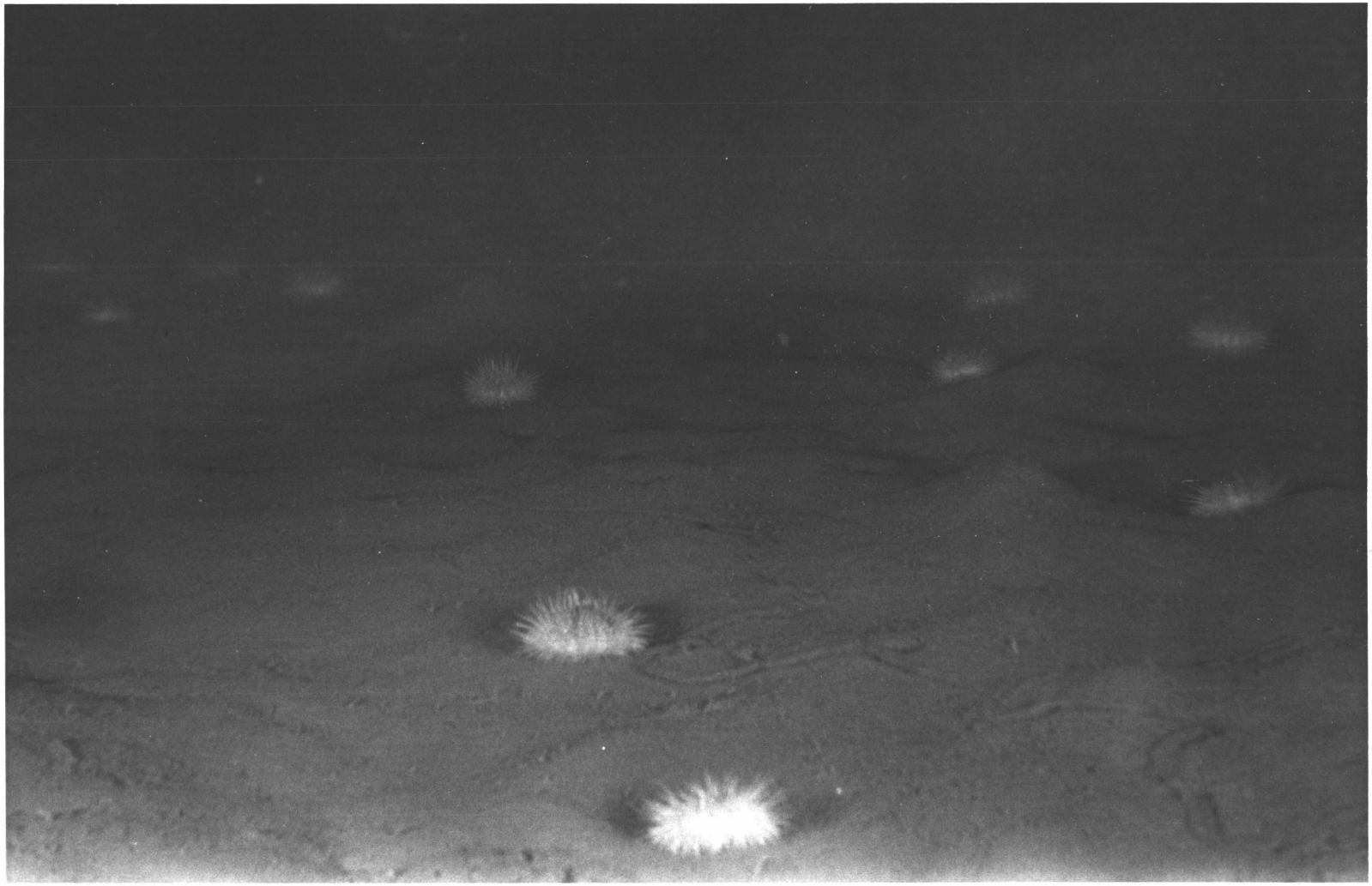

Figure II-4

available, it is difficult to define a characteristic height or spacing for these features. Although we have no reason to expect significant differences along the 200 m isobath, especially in light of the similar sediment texture, we cannot demonstrate that these features are representative of roughness elements in our area of study. We can only state that the types of features in these photos could be responsible for the presence of the form drag which we infer from our current data.

Techniques Used to Estimate Bed Stress

It is common practice in sediment-transport studies to measure the mean current some distance above the bed (typically 100 cm) and to estimate the bed stress from the quadratic law:

$$\tau_b = C_{100}\rho[\bar{U}(100)]^2 \qquad (12)$$

Here τ_b is taken to be the bed stress, and C_{100} is a dimensionless drag coefficient (Sternberg, 1968, 1972; McCave, 1973; Ludwick, 1975; Komar, 1976). Because C_{100} is commonly determined by a logarithmic profile technique in which the velocity profile is measured well above the bed, the measured stress and therefore the calculated C_{100} may be influenced by form drag. If the goal of a study is to obtain an estimate of skin friction for use in entrainment or transport calculations, and if form drag is significant, use of (12) may yield τ_b considerably larger than the stress influencing the near-bed sediment transport. The same statement can obviously be made about Reynolds stress estimates if based on measurements a significant

distance from the bed. The above ideas are not new but rather are consequences of concepts presented most recently by Smith (1977), Smith and McLean (1977). Our experiment, however, provides the first, though somewhat limited, data set from the ocean which demonstrates the degree to which the local bed stress may be overestimated. Were it not for our measurements within 15 cm of the bed, our measurements of U_* from the upper portion of our profiles would have been assumed to represent the friction velocity at the bed, and the relatively large Z_o values from the upper portion of the profiles might have been interpreted to imply that the flow was not hydrodynamically smooth and that a viscous sublayer did not exist. In contrast, our data clearly demonstrate that the above assumptions cannot be justified without evidence from velocity profiles closer to the sediment. For example, the calculation by Weatherly and Wimbush (1980) of $U_* = 0.66$ cm/s and $Z_o = 0.49$ cm based on profiles obtained with sensors located between 18 cm and 565 cm above the sediment does not necessarily indicate that a viscous sublayer did not exist or that the $U_* = 0.66$ cm/s value represents the skin friction or the stress at the bed. Without near-bed velocity profiles it is difficult to evaluate their conclusion that the critical erosion stress ($u_* = 0.6$ cm/s) was exceeded, particularly because of the possible influence of the current ripples shown in their Figure 2.

Although the flow during our experiment was hydrodynamically smooth in the sense that a viscous sublayer did always exist, drag coefficients computed from the extrapolated velocity at 100 cm (using the U_* values for the upper logarithmic layer) fall within the range

other workers cite as typical for hydrodynamically rough flow. For example, the data of Sternberg (1972) yield values of C_{100} which, for fully rough flow, lie between 10^{-3} and 10^{-2} with a mean of 3.1×10^{-3}, while the data in Weatherly and Wimbush (1980) can be used to calculate a value of 5.6×10^{-3} for C_{100}. The important conclusion suggested by our data is that determinations of large Z_o values and large C_{100} values, if not derived from data just above the sediment-water interface, may reflect the influence of form drag on the boundary layer flow, and use of these values in calculating the bed stress may significantly overestimate the actual stress at the bed. In Table 4 we present the ratio of the "total stress" (τ_t), calculated from the upper portion of our velocity profiles, to the stress at the bed which was determined by viscous sublayer measurements and the use of (4). Entrainment or near-bed transport calculations based on velocity profile (or Reynolds stress) measurements taken more than 15 cm above the bed would in this case have been based on stress estimates more than four times too large.

How Representative is Our Data?

It must be emphasized that the data which form the basis for this paper were obtained during one experiment conducted at 199 m water depth on the Oregon shelf during October 1978 and can only be assumed to reflect the flow conditions during this experiment. While form drag may be of equal (or greater) importance in other shelf and deep-sea locations, we lack the direct evidence necessary to demonstrate this. In our subsequent experiments (April and June, 1979),

Table 4. Ratio of the total stress (τ_t) to the bed stress (τ_b). Also shown are drag coefficients (C_{100}) calculated using the data from the upper logarithmic region.

Data Interval	$\bar{U}(100)$ (cm/s)	u_* (sublayer) (cm/s)	U_* (upper region) (cm/s)	C_{100}	$\frac{\tau_t}{\tau_b}$
1	9.1	.27	.62	4.7×10^{-3}	5.3
2	6.6	.30	.62	8.8×10^{-3}	4.3
3	17.8	.51	1.00	3.2×10^{-3}	3.8
4	15.0	.47	1.02	4.6×10^{-3}	4.8
5	6.8	.19	.62	8.2×10^{-3}	10.6

we restricted the profiler motion to 6 cm in order to increase our resolution of the viscous sublayer and so-called buffer layer. While doing so had the additional benefit of allowing us to construct mean velocity profiles using averaging times as short as 10 minutes, it now prevents us from examining these profiles for evidence of form drag. It is important to note, however, that data from the sublayer profiler coupled with data from a Savonius rotor 59 cm above the sediment during the June 1979 experiments (in 90 m and 180 m water depths) are consistent (within the accuracy of the rotor) with the assumption of a constant stress layer extending from the sediment up to 59 cm (Chriss and Caldwell, 1981b). The above data suggest that form drag may not have significantly influenced the flow during the June 1979 experiment.

Clearly, future experiments must incorporate both sublayer profiling (to determine bed stress) as well as adequate profiling of the lower logarithmic region in order to determine the extent to which bottom boundary layer flow is influenced by form drag in various environments.

CONCLUSIONS

Above the viscous sublayer, the velocity profiles observed during this experiment consisted of two distinct regions, each characterized by a different logarithmic velocity profile. Applying the models of Elliot (1958) and Arya (1975a) to this data, we conclude that the influence of form drag on boundary layer flow over sparse roughness elements could produce the velocity structure which we have

observed. When form drag is significant, the use of the logarithmic profile or Reynolds stress techniques, if based on flow measurements obtained more than a few tens of centimeters from the bed, may yield stress estimates several times larger than the bed stress. If the goal of a study is to obtain bed stress estimates for use in sediment transport or entrainment calculations, such errors may be unacceptable.

Large values of the roughness parameter (Z_o) and the drag coefficient (C_{100}), if based on measurements at substantial distances above the bed, do not rule out the existence of a viscous sublayer at the sediment-water interface. This observation is significant, not only for sediment and momentum transport problems, but also because the presence or absence of a viscous sublayer may have important implications for the vertical transport of heat and chemical species at the sediment-water interface.

CHAPTER III

TURBULENCE SPECTRA FROM THE VISCOUS SUBLAYER AND BUFFER LAYER AT THE OCEAN FLOOR

T. M. Chriss

School of Oceanography

Oregon State University

Corvallis, Oregon 97331

Submitted to Journal of Fluid Mechanics

ABSTRACT

An experiment conducted in June 1979 on the Oregon shelf has yielded the first measurements of velocity fluctuations in the viscous sublayer and buffer layer of a geophysical boundary layer flow. The scaling proposed by Blakewell and Lumley (1967) for the viscous sublayer has been tested and found to work remarkably well in collapsing spectra from both geophysical and laboratory flows. Buffer layer spectra collapse reasonably well with laboratory spectra when scaling similar to that normally used in the logarithmic layer is applied to the buffer layer.

1. Introduction

One of the basic premises in the study of boundary layer turbulence is that measurements of mean and fluctuating quantities in boundary layer flows can be reduced to "universal forms" when non-dimensionalized by characteristic length and velocity scales (Monin and Yaglom, 1971, chapter 3). In an earlier study (Chriss and Caldwell, 1981b) we examined the hypothesis that the mean flow near the viscous sublayer of the bottom boundary layer on the Oregon continental shelf can be described as a universally similar, neutrally-buoyant boundary layer flow on a smooth wall. We concluded that, although the thickness of the viscous sublayer scales with ν/u_* as required by the concept of universal similarity, the scaling was not exact and the very near-bed flow is not quite so simple as neutrally-buoyant, smooth-wall turbulent boundary layer flows in the laboratory. (Here u_* is the friction velocity and ν is the kinematic viscosity.)

In this paper, we examine velocity spectra from a similar experiment in order to evaluate the hypothesis that spectra from the viscous sublayer and buffer layer of smooth-walled laboratory and geophysical flows can be reduced to universal spectral forms by suitable non-dimensionalization. In addition, we examine the hypothesis that the profile of non-dimensional velocity fluctuations in the viscous sublayer at the ocean floor is the same as that found in the laboratory.

2. The Experiment

The experiment was carried out on June 9-10, 1979 in 185 m water depth at 45°20'N on the Oregon continental shelf. The surface sediment is a silty sand (Runge, 1966). The data were obtained from profiling heated thermistor velocity sensors mounted on a 2 m high tripod placed on the sea floor. A digital data acquisition system on the tripod sampled each thermistor once every 2 seconds. Additional instrumentation on the platform included temperature sensors, Savonius rotors and a time-lapse motion picture camera which monitored the condition of the sensors.

Current was supplied to each thermistor to heat it approximately 20°C above the water temperature. The temperature achieved by the thermistor depends on the power dissipated in it and on the heat transferred away from the probe by the surrounding fluid. Because the calibration is a function of the water temperature and the orientation of the flow with respect to the thermistor, each thermistor was post-calibrated at the temperatures and flow directions observed during the experiment. The calibrations were performed by towing the thermistors in a 1 m radius annular channel. The power dissipated in the thermistor per unit change in temperature was related to the flow velocity by

$$P/\Delta T = a + bU^N \qquad (1)$$

where P is the power dissipated in the thermistor, ΔT is its temperature rise, U is the flow velocity, and a, b, and N are experimentally

determined. Inversion of this relationship allows the determination of current speed from values of $P/\Delta T$ computed from the output of the circuit. With this procedure, current speed can be determined with better than 0.1 cm s^{-1} accuracy in the laboratory. The frequency response of these thermistors as velocity sensors has not been determined, but the same thermistors (Thermometrics P85 thermistors) have a -3 db point of 7 Hz when used as temperature sensors (Dillon and Caldwell, 1980). Because self-heated thermistors have faster response times when used as velocity sensors, the frequency response of the velocity sensor was at least 7 Hz, far higher than necessary to resolve the Nyquist frequency, 0.2 Hz. The heated thermistors are used to determine the current speed only. Current direction is indicated by a small stationary vane.

The heated thermistors were mounted on a profiling arm carried up and down by a crank-and-piston mechanism driven by an underwater motor. The profiler mechanism was mounted outside one of the tripod legs, assuring unobstructed flow through an arc of 300 degrees. Only those time intervals when the flow was unobstructed were chosen for analysis. The profiling period for this experiment was 213 minutes. The total vertical travel of the sensors was 6 cm. To make sure that the thermistors penetrated the viscous sublayer (which was at most a few cm thick), we allowed the thermistors to penetrate the sediment at the bottom of each profile. The vertical position of the thermistors was determined by a potentiometer connected to the profiler motor. Calibration of the profiler system using a dial indicator showed that the vertical position of the arm can be determined within

0.03 cm. The position of the sediment-water interface was taken to be the zero-velocity intercept of the (linear) velocity profile within the viscous sublayer.

3. Data Analysis

The data which form the basis of this study were obtained from two heated thermistors separated horizontally by 11 cm and offset approximately 0.5 cm in the vertical direction. The thermistors penetrated the sediment by 4.5 and 5 cm, so we have current measurements from the region between the boundary and 1.5 cm above the boundary. Based on the friction velocities ($u_* = (\tau_o/\rho)^{1/2}$ which ranged from 0.14 cm s^{-1} to 0.36 cm s^{-1}, sensor positions at the very top of the profile correspond to non-dimensional wall distances ($y^+ = yu_*/\nu$) which range from $y^+ = 9$ to $y^+ = 29$. The time required for the sensors to traverse from the very top of the profile to the boundary was 2200 seconds. Because of the crank-and-piston nature of the profiler mechanism, vertical traverse speeds were slowest in the top millimeter of the profile (approximately 2.1×10^{-4} cm s^{-1}) and most rapid near the sediment (approximately 1.2×10^{-3} cm s^{-1}). At these speeds it required 400 to 700 seconds for the sensors to traverse the viscous sublayer between $y^+ = 0$ and $y^+ = 6$. Figure 1 shows typical time series in the viscous sublayer and in the buffer layer which separates the viscous sublayer from the overlying logarithmic layer.

For each upward or downward traverse, a mean profile for the viscous sublayer was constructed by averaging the velocity measure-

Figure III-1. Typical time series from the viscous sublayer (lower series) and buffer layer (upper series). The series shown are not simultaneous. During the course of the sublayer series, the sensor moved from $y^+ = 6$ to $y^+ = 1$, accounting for the decrease in mean velocity. During the buffer layer series, the sensor moved from $y^+ = 22$ to $y^+ = 18$.

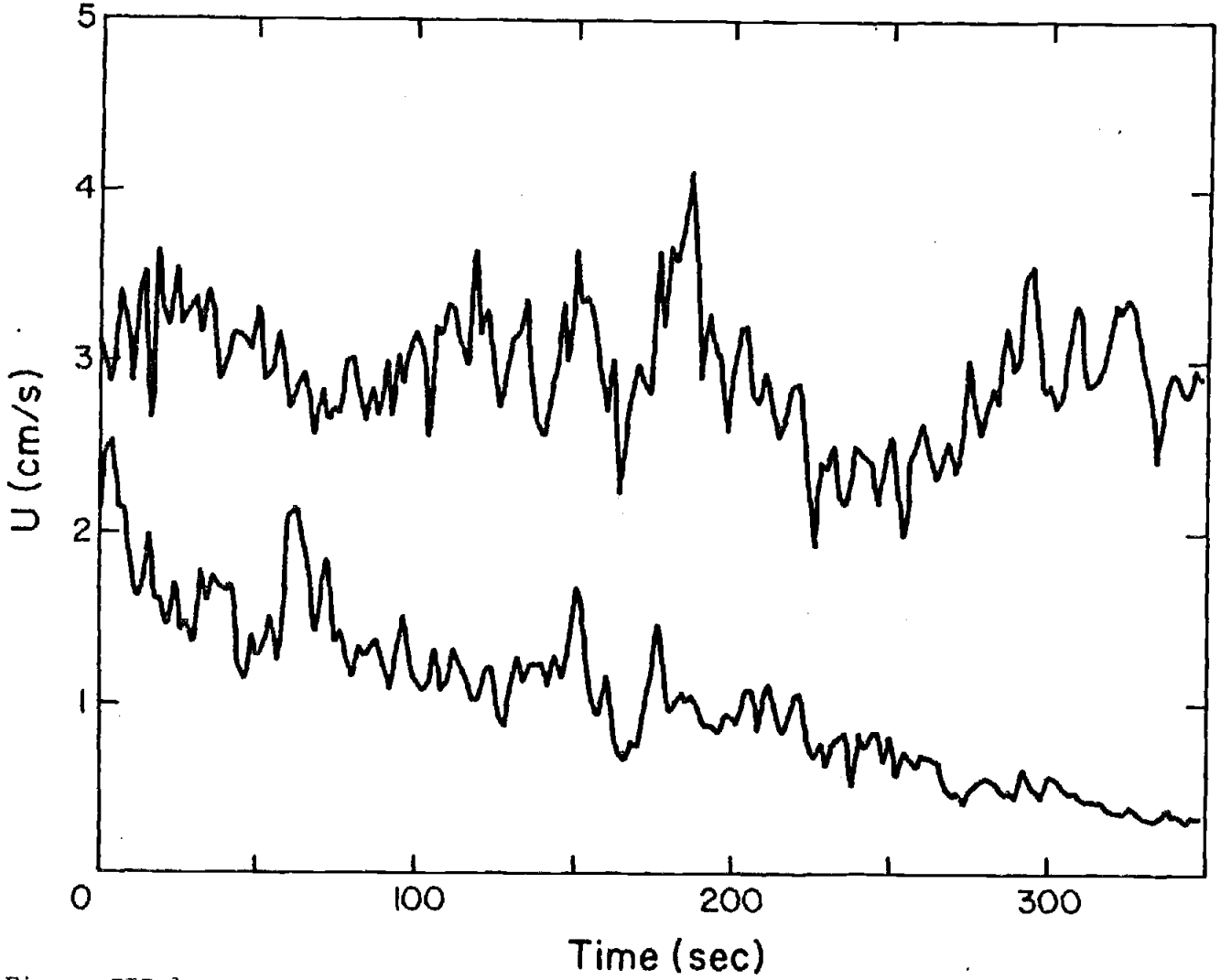

Figure III-1.

ments over vertical intervals of approximately 0.05 cm (Fig. 2). The velocity shear in the sublayer was then used to compute the bed stress (τ_o) by

$$\tau_o = \rho\nu \frac{\partial \bar{U}}{\partial y} \qquad (2)$$

where ρ and ν are the density and kinematic viscosity of the fluid. The friction velocity calculated from the bed stress was later used in the non-dimensionalization of the spectra.

4. Spectra from the viscous sublayer

Although the output of the heated thermistor circuitry does not indicate the current direction, the energy in our computed current spectra is dominated by the contributions of the streamwise velocity fluctuations. Given the magnitude of the mean flow and estimates of the typical magnitude of vertical and cross stream velocity fluctuations in the viscous sublayer and buffer layer of laboratory flows (see, for example, Eckelmann, 1974), it can be shown that, because of the nature of the vector addition process, the sensor responds almost exclusively to the streamwise component of the velocity fluctuations. At most a few percent of the energy in our spectra is due to cross-stream contributions.

Ideally, the spectra for the viscous sublayer would have been computed over long time intervals with the sensors located at a fixed y^+. But because of the self-contained nature of the instrumentation, we could not adjust the sensor positions once the platform left the

Figure III-2. Typical mean velocity profile. The straight line represents a linear fit to the data in the viscous sublayer.

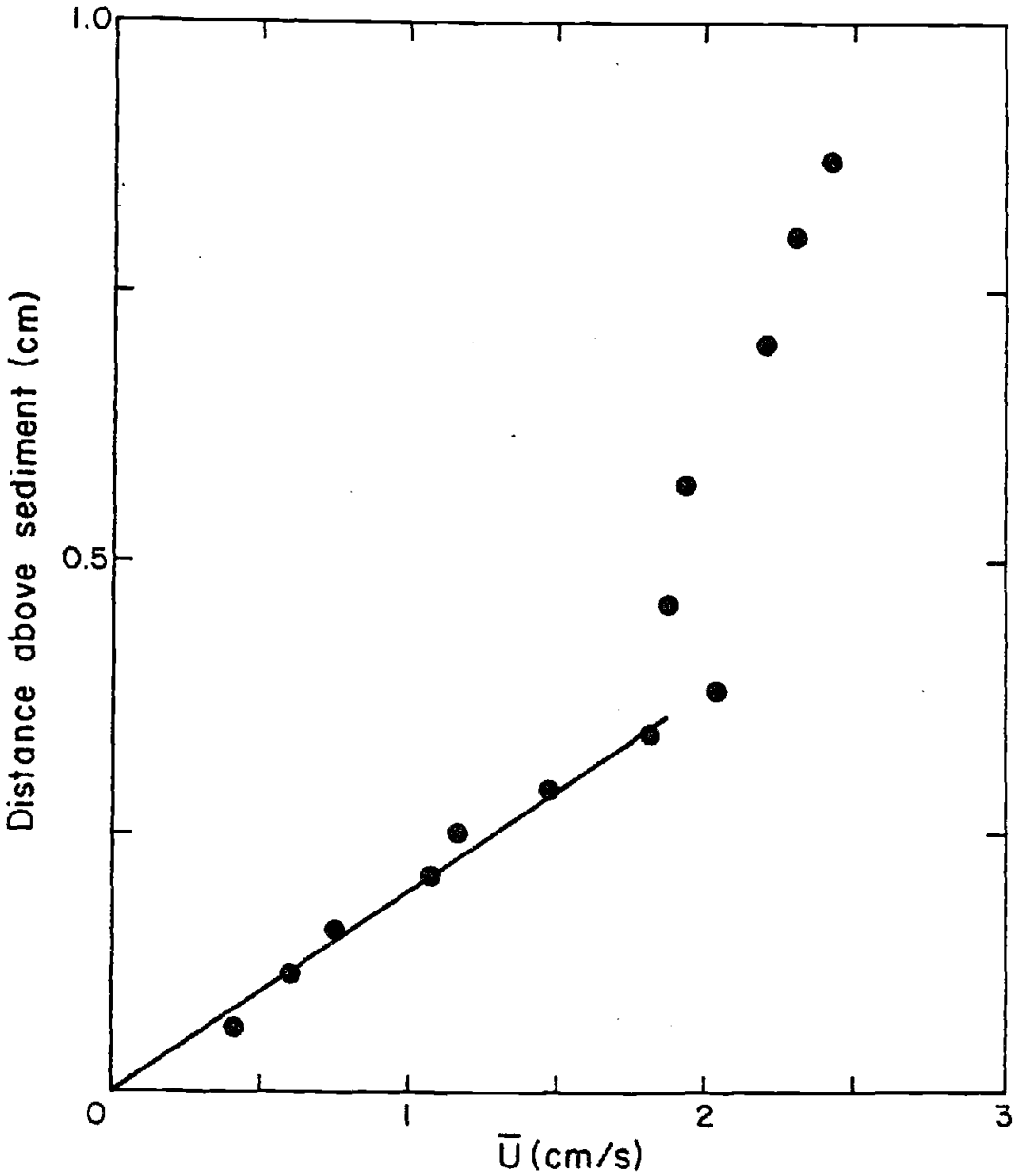

Figure III-2.

deck of the ship. Because of this inability to precisely set the position of the sensors with respect to the boundary (due to platform settling, etc.) and because of the need to determine the shear in the sublayer (to obtain u_*), we allowed the sensors to move slowly through the sublayer hoping that this slow change of y^+ would not seriously influence the resulting spectra. If the spectral scaling suggested by Blakewell and Lumley (1967) is applicable, the shapes of our sublayer spectra (determined from the slowly moving sensor) should not differ from those from a fixed sensor.

The sublayer spectra were computed for 128-point series. The series chosen were those for which the sensors were located in the linear profile characteristic of the region where momentum transport is dominated by viscosity. During the 256 second time interval over which the spectra were computed, the sensor moved 0.2 to 0.3 cm, a y^+ change of approximately 2 to 4. Prior to spectral analysis, the series were detrended to remove the effect of the velocity gradient. Power spectral densities (SD(f)) defined by

$$u'^2 = \int_0^\infty SD(f)\,df \qquad (3)$$

were computed using a fast Fourier transform algorithm. In (3), u' is the r.m.s. value of the streamwise velocity fluctuation. After computation, the raw spectral estimates were band averaged.

Typical sublayer spectra are shown in Figure 3. Blakewell and Lumley (1967) and Ueda and Hinze (1975) present spectra from the viscous sublayer of laboratory flows in which the fluids and the flow conditions were significantly different from those in the ocean.

Figure III-3. Typical spectra from the viscous sublayer. Confidence intervals are the same as those shown in Figure III-4.

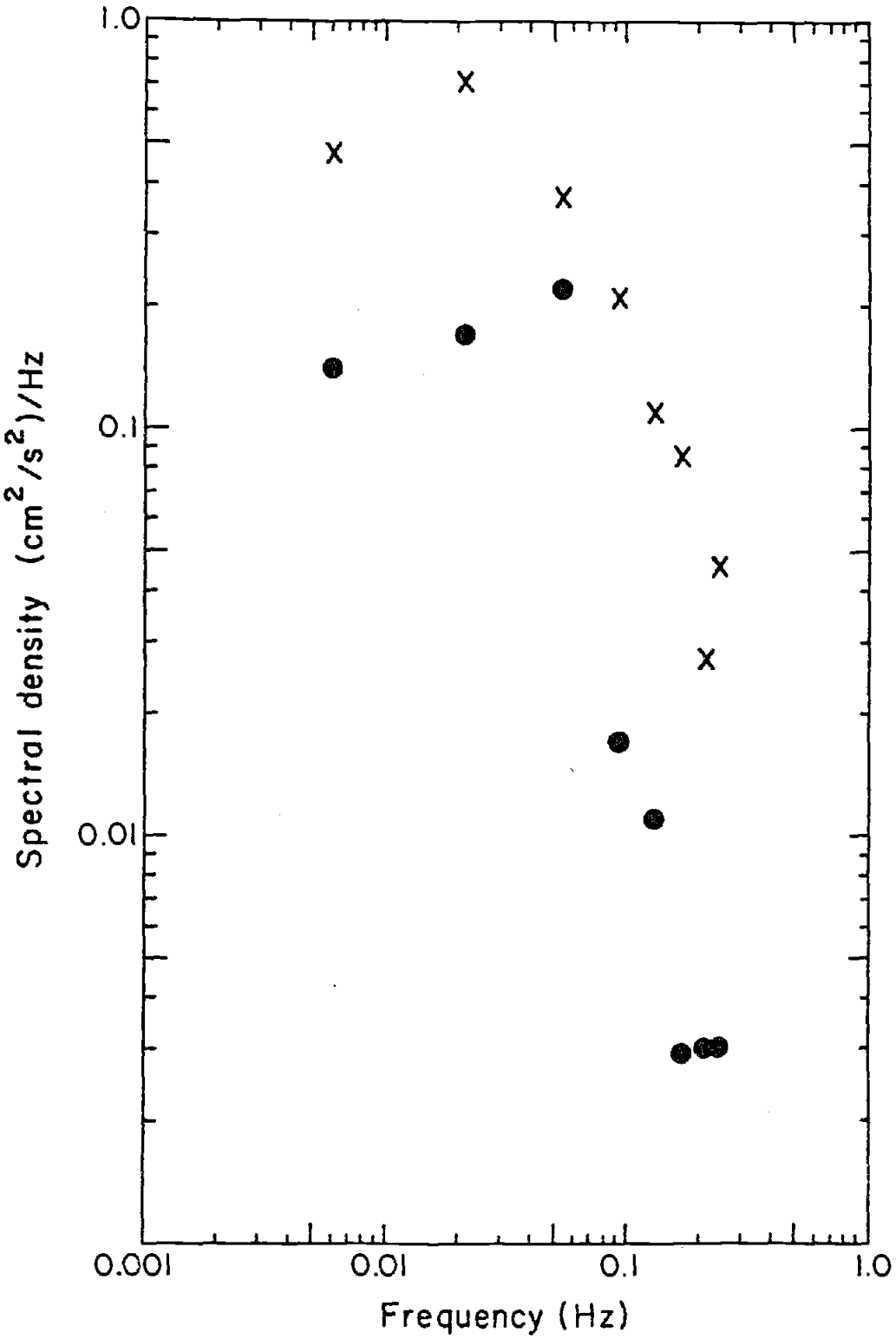
1.0
0.1
0.01
Spectral density (cm²/s²)/Hz
0.001
0.01
0.1
1.0
Frequency (Hz)

Figure III-3.

Blakewell and Lumley's data are from a turbulent pipe flow using glycerine (ν = 2.18 cm^2 s^{-1}) as the fluid, whereas the Ueda and Hinze data are from a wind tunnel (ν = 0.151 cm^2 s^{-1}). The friction velocities were 50 cm s^{-1} and 39.1 cm s^{-1}, respectively. The unscaled spectra from these studies are quite different from those of our study (Fig. 4). It should be mentioned that computational errors apparently crept into the spectral plots presented in both laboratory studies. The spectra presented by Blakewell and Lumley integrate to approximately 2π times the total variance of the series (which can be determined from other figures in the paper), while those presented by Ueda and Hinze integrate to 76 times the variance. Because spectra by the normal definition must integrate to the variance, we have adjusted the spectral densities of the two laboratory studies by dividing by 2π and 76, respectively.

Blakewell and Lumley propose that sublayer spectra can be reduced to a single curve if frequencies ($\omega = 2\pi f$) are non-dimensionalized by (ν/u_*^2) and spectral densities are non-dimensionalized by ωy^2, where y is the dimensional distance from the wall. Data presented in their paper support the proposed scaling to the extent that the spectra from three different y^+ positions within the sublayer are collapsed by this scaling to a single curve. Because u_* and ν were not varied in Blakewell and Lumley's experiment, the collapse of their spectra to a single curve does not imply that the scaling of frequency is correct. A test of the frequency scaling requires data from flows in which u_*^2/ν varies significantly. Based on the viscosity of sea water (0.015 cm^2 s^{-1}) and the range of u_* in our experiment,

Figure III-4. Sublayer spectra from our study (at left) plotted with sublayer spectra from the laboratory studies of Blakewell and Lumley (1967) and Ueda and Hinze (1975). The Blakewell and Lumley spectra are for $y^+ = 1.25$ (X) and $y^+ = 5$ (□). The Ueda and Hinze spectrum (●) is for $y^+ = 3$. Confidence limits shown for our spectra are 95% confidence limits assuming a chi-square distribution (Bath, 1974).

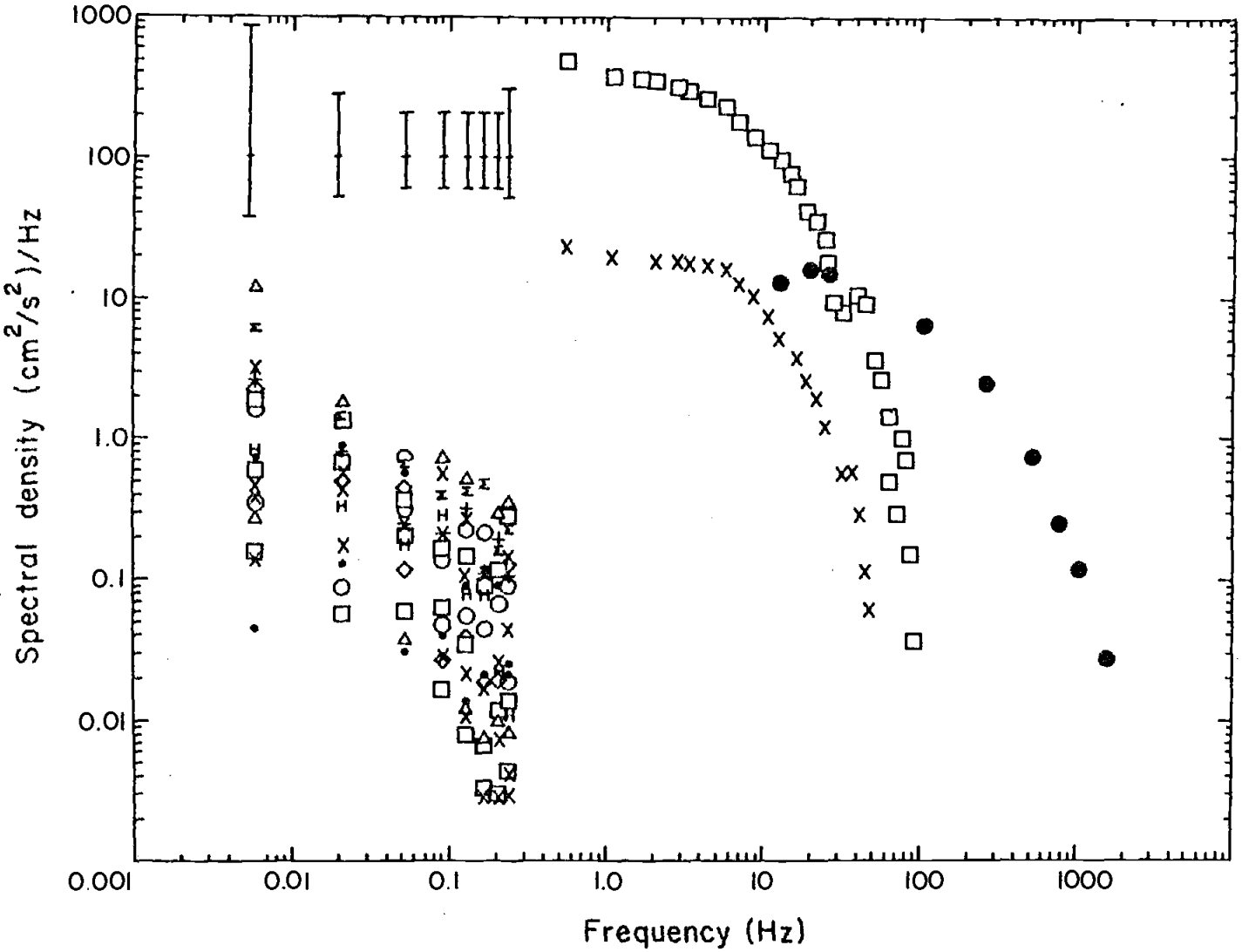
1000
100
10
1.0
0.1
0.01
0.001
0.01
0.1
1.0
10
100
1000
Spectral density (cm²/s²)/Hz
Frequency (Hz)

Figure III-4.

ν/u_*^2 is up to 470 times larger than in Blakewell and Lumley's experiment and up to 11,000 times larger than in the Ueda and Hinze experiment. The spectra from the three experiments thus furnish an excellent opportunity to test the scaling proposed by Blakewell and Lumley.

Before applying the proposed scaling, we return to a question considered earlier: the effect of the traversing of the sensor on the computed power spectrum. Consider a situation in which u_* is constant over the time interval used to compute the spectrum. If the scaling proposed by Blakewell and Lumley holds, then for fixed ν and u_*, the non-dimensional spectral density ($\hat{SD} = SD(\omega)/y^2\omega$) depends only on the non-dimensional frequency ($\hat{\omega} = \omega\nu/u_*^2$). Thus, with fixed ν and u_*, the dimensional spectral density ($SD(\omega)$) at dimensional frequency ω should be equal to $c(\omega)y^2$ where $c(\omega)$ is a proportionality constant depending only on ω. Thus, a sensor moving at a constant traverse velocity from $y = y_1$ to $y = y_2$ should observe a spectral density at frequency ω given by

$$SD(\omega) = 1/(y_2 - y_1) \int_{y_1}^{y_2} c(\omega)y^2 \, dy \qquad (4)$$

which is equivalent to $c(\omega)y_3^2$ where y_3 is given by

$$y_3^2 = \frac{y_2^3 - y_1^3}{3(y_2 - y_1)} \qquad (5)$$

So, if the scaling proposed by Blakewell and Lumley is valid, the spectrum calculated from a time series obtained from a sensor which moves from y_1 to y_2 should be identical to the spectrum which would have been obtained from a fixed sensor at y_3 (providing that the

time series had first been detrended to remove the variance resulting from traversing through a mean velocity gradient). In scaling our spectra, we have used the lowermost and uppermost positions of the thermistor during the spectral time interval to determine the value of y_3 to use in the non-dimensionalization of the spectral density.

In Figures 5 and 6, we present scaled versions of the spectra of Figure 4. Although the result is not perfect, the scaled spectra from the three studies agree remarkably well. Much of the scatter at the low frequency end of our data may reflect the fact that each point represents a single spectral estimate and so the uncertainty is large. Ensemble-averaged spectra from our experiment (Fig. 7) compare very well with the laboratory spectra except within the non-dimensional frequency range of 0.01 to 0.08 where our spectra show slightly less energy.

The agreement of the non-dimensional spectra from the three experiments (Fig. 7) is strong support for the validity of the scaling proposed by Blakewell and Lumley. Despite the potentially greater complexity of the geophysical boundary layer flow, the viscous sublayer at the ocean floor behaves remarkably like its laboratory equivalent.

Figure III-5. Scaled sublayer spectra from Blakewell and Lumley (1967) and Ueda and Hinze (1975). Symbols are the same as in Figure III-4.

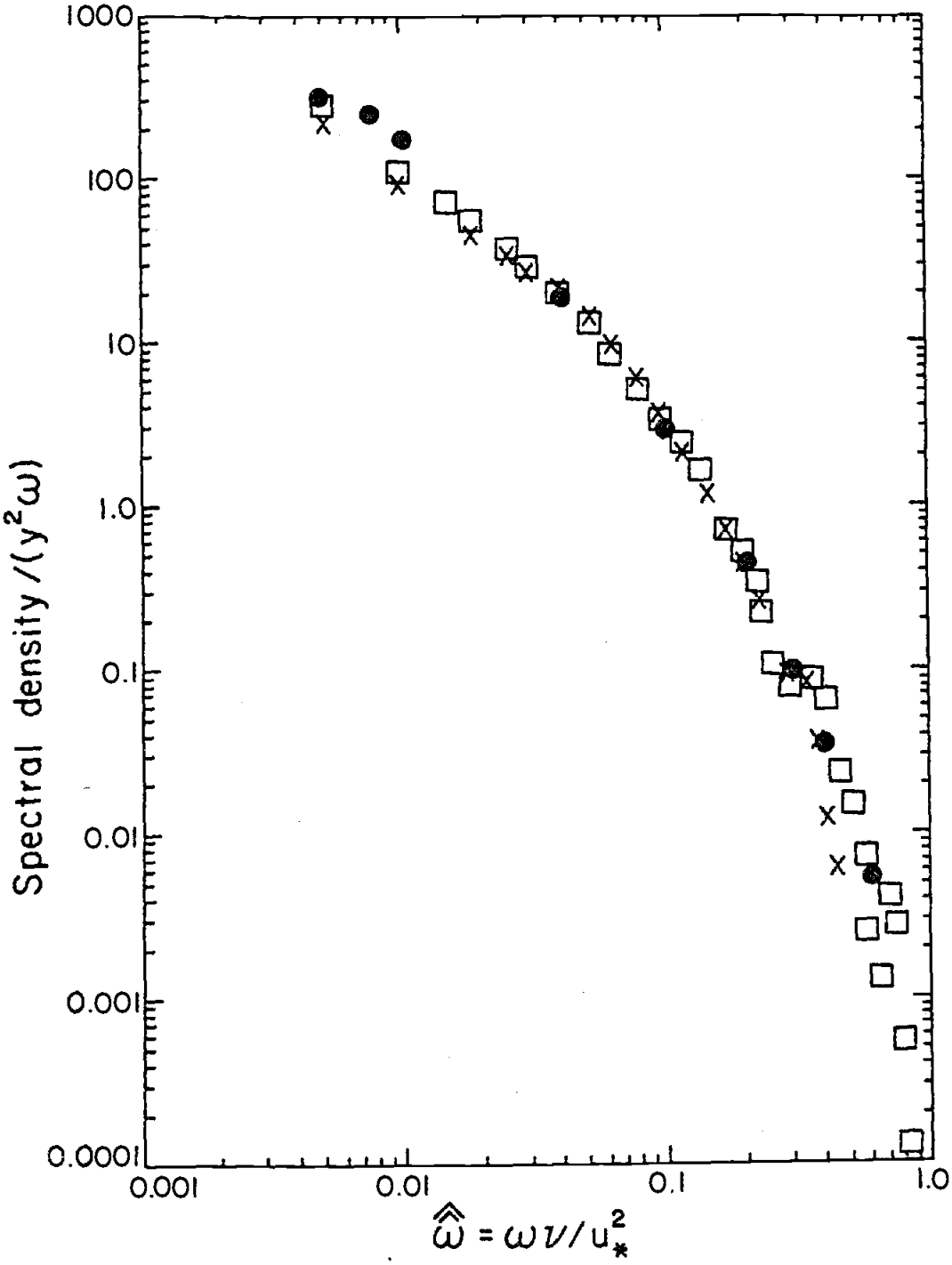
1000
100
10
1.0
0.1
0.01
0.001
0.0001
0.001
0.01
0.1
1.0
Spectral density /(y²ω)
ω̂ = ων/u*²

Figure III-5.

Figure III-6. Scaled spectra from our study together with those of the two laboratory studies. In this figure, all laboratory points are shown by solid circles.

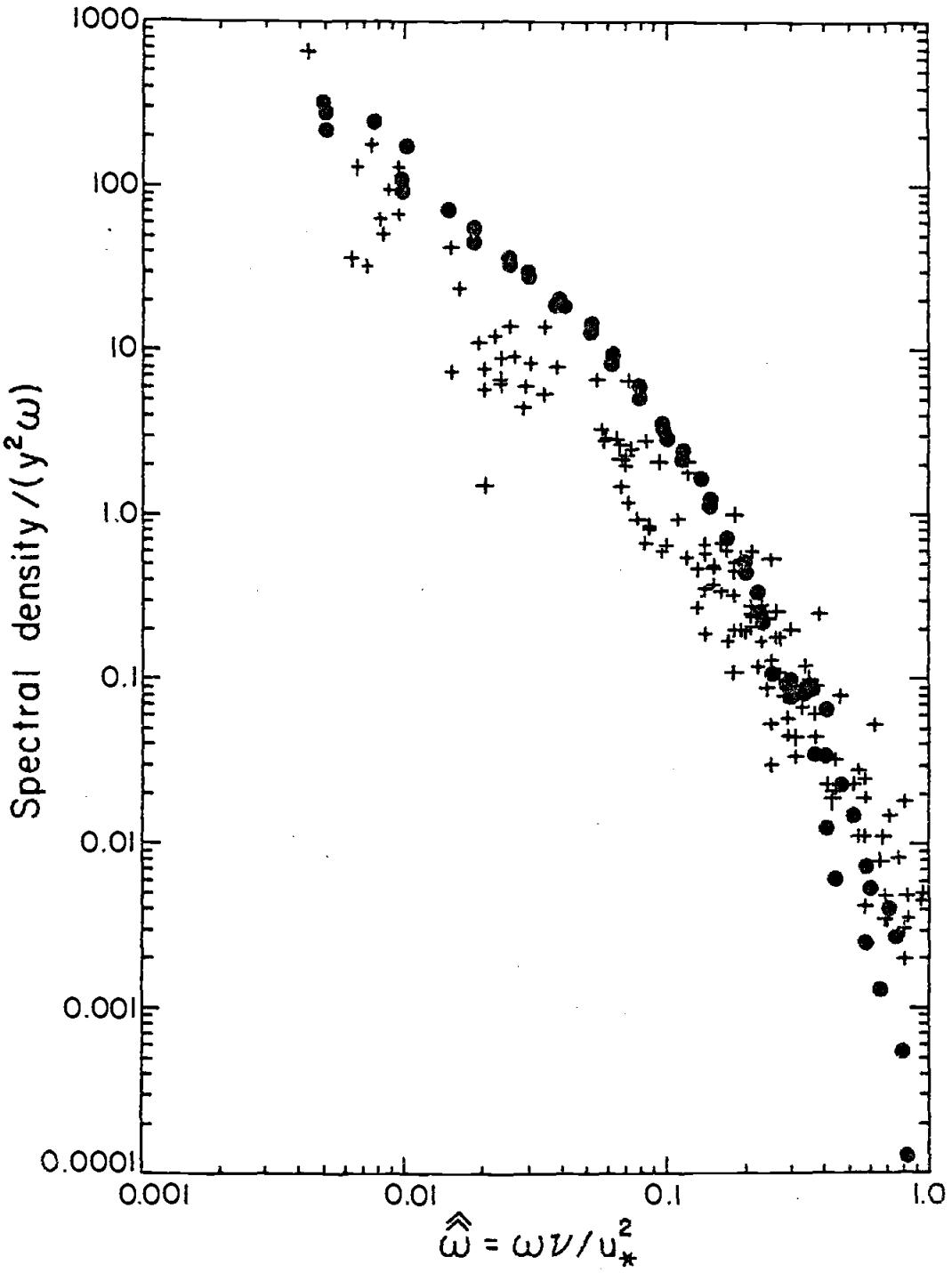
1000
100
10
1.0
0.1
0.01
0.001
0.0001
0.001
0.01
0.1
1.0
Spectral density /(y²ω)
ω̂̂ = ων/u*²

Figure III-6.

Figure III-7. Ensemble-averaged spectrum from our study (■) plotted with the laboratory spectra (o). The spectral estimate for the lowest frequency is based on only one data point in the averaging band and therefore is not as well determined as the other estimates. The horizontal arrows delimit the energy containing range of the laboratory spectra.

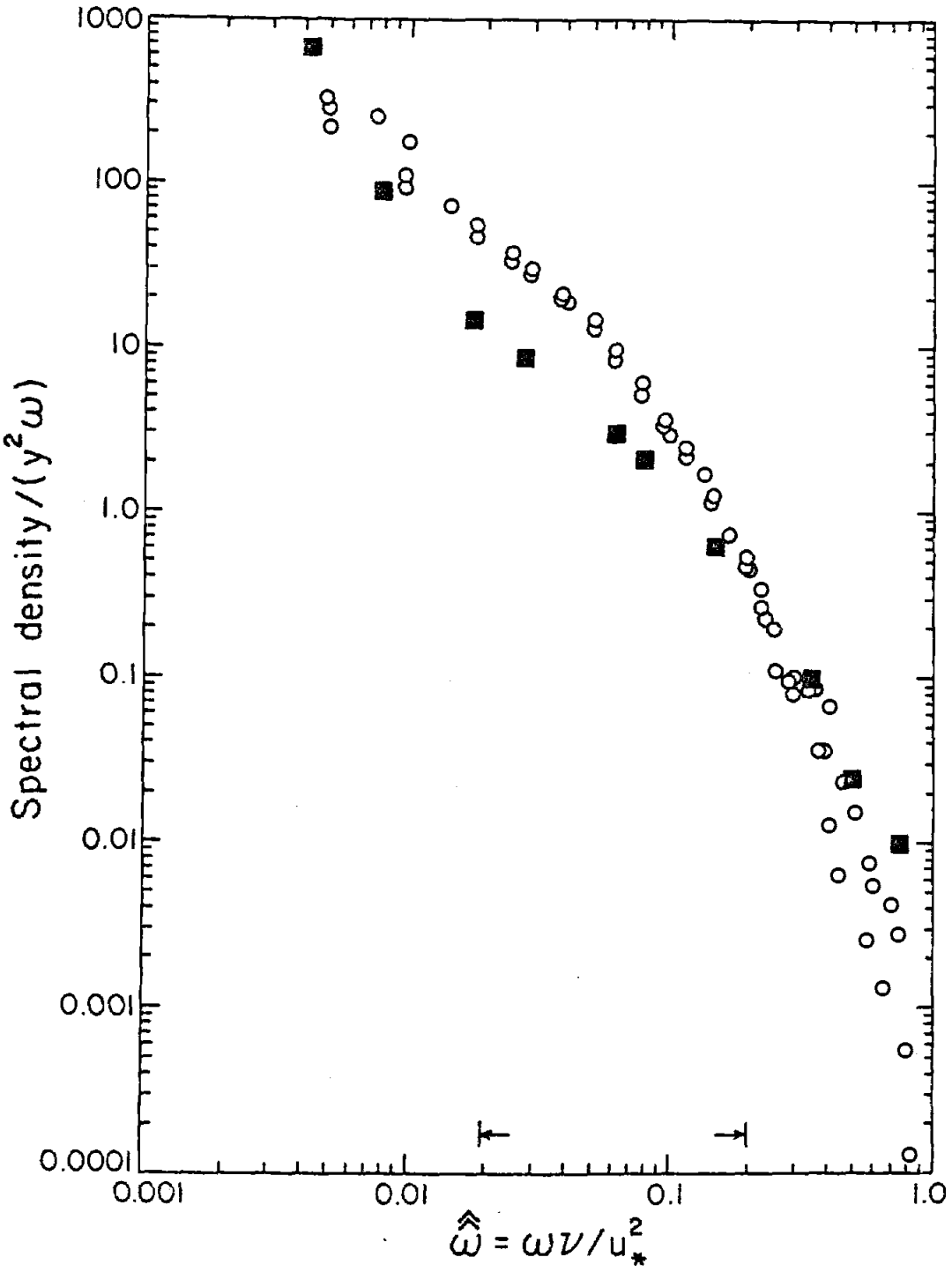
1000
100
10
1.0
0.1
0.01
0.001
0.0001
0.001
0.01
0.1
1.0
Spectral density/($y^2\omega$)
$\hat{\hat{\omega}} = \omega\nu/u_*^2$

Figure III-7.

5. The vertical structure of the streamwise velocity fluctuations in the viscous sublayer

A number of laboratory studies, while not always determining the frequency dependence of the streamwise velocity fluctuations, have examined the dependence of the r.m.s. streamwise velocity fluctuation (u') on y^+ (Eckelmann, 1974; Mitchell and Hanratty, 1966; Hanratty, 1967; Ueda and Hinze, 1975; Kreplin and Eckelmann, 1979). The laboratory data suggest that u'/u_* is roughly proportional to y^+ between $y^+ = 1$ and $y^+ = 5$. The value of the proportionality constant, however, varies from study to study. Mitchell and Hanratty (1966) summarize early determinations of the "constant" (Laufer, 1951, 1954; Klebanoff, 1954) which show tremendous variability in its value (from 0.21 to 0.44), but more recent determinations (Mitchell and Hanratty, 1966; Blakewell and Lumley, 1967; Hanratty et al., 1977; Ueda and Hinze, 1975; Eckelmann, 1974; Kreplin and Eckelmann, 1979) all yield values between 0.32 and 0.38 in the region between approximately $y^+ = 1$ and $y^+ = 5$. The data of Kreplin and Eckelmann suggest that the value of the "constant" varies with y^+ and decreases from 0.38 at $y^+ = 4.5$ to 0.32 at $y^+ = 1.5$. Using flush-mounted hot-film wall sensors, Eckelmann (1974), Kreplin and Eckelmann (1979), and Sreenivasan and Antonia (1977) obtained estimates of 0.24 to 0.25 for the limiting value of the constant at the wall, although Py (1973) and Fortuna and Hanratty (1971) using different types of wall mounted sensors obtained 0.3 at the wall. Because the limiting value of the constant is equal to the ratio of the r.m.s. fluctuating wall stress to the mean wall stress,

its value may be relevant in sediment transport studies.

We have determined u' for each of the 128-point sublayer time series. Based on 17 intervals we find $u'/(u_* y^+)$ to be 0.20 ± 0.03 (standard deviation). To resolve 99% of the variance in Blakewell and Lumley's sublayer spectrum, the spectra must include the non-dimensional frequency band from approximately 4.6×10^{-3} to approximately 4.2×10^{-1}. Although the ensemble average of our spectral data (Fig. 7) resolves this energy-containing band, each individual 128-point spectrum does not. Depending on the value of the friction velocity u_*, each 128-point spectrum missed predominantly either the high frequency or the low frequency portion of the energy-containing range. Given the lowermost and uppermost non-dimensional frequencies resolved in each spectrum, and using the Blakewell and Lumley spectrum as a standard, we find that each spectrum resolved from 76% to 90% of the expected variance of the streamwise velocity fluctuations. Thus, the ratio of $u'/(u_* y^+)$ calculated from our data is likely to be too low. After using the Blakewell and Lumley spectrum to correct for these effects, $u'/(u_* y^+)$ becomes 0.21 ± 0.03. Even after correction, our sublayer spectra contain less energy than equivalent spectra from the laboratory.

6. Spectra from the buffer layer

The buffer layer spectra were computed for 256-point series, selected so that the sensor was within the top millimeter of the traverse and y^+ was greater than 18. For these intervals y^+ varied

from 18 to 29, depending on u_*. With the very slow traverse speeds at the top of the profile, the sensors moved only 1 to 1.2 non-dimensional units during the 512 seconds over which a spectrum was computed. Laboratory data suggest little change in the turbulence structure over this small distance, so the profiler motion should not influence the buffer layer spectra. To remove the potential effect of a temporal trend in mean velocity, the series were detrended prior to analysis.

Figure 8 shows several representative buffer layer spectra (y^+ = 19 and y^+ = 29) from our study, along with buffer layer spectra (y^+ = 20 and y^+ = 21) from Blakewell and Lumley (1967) and Ueda and Hinze (1975). No spectral scaling has been proposed for buffer layer velocity spectra. Because u'/u_* varies by no more than 30 percent over the range y^+ = 18 to y^+ = 30 (Blakewell and Lumley, 1967; Kreplin and Eckelmann, 1979; Ueda and Hinze, 1975), Blakewell and Lumley's spectral scaling for the viscous sublayer (which depends strongly on y^2) cannot possibly work for buffer layer spectra. Thus, we sought some other scaling which might be successful. In the logarithmic layer of atmospheric and laboratory boundary layer flows, it is traditional to non-dimensionalize the frequency axis by $y/\bar{U}(y)$ (where $\bar{U}(y)$ is the mean velocity) and to non-dimensionalize the spectral densities by u_*^2/ω. We have applied this scaling to the two sets of laboratory data (Fig. 9). Rather than dividing the spectral density by u_*^2/ω as is commonly done, we have divided by $u_*^2\ \hat{\omega}/\omega$, where $\hat{\omega}$ is the non-dimensional frequency. This non-dimensionalization is not fundamentally different, but has the advantage that the shape of the

Figure III-8. Typical buffer layer spectra from our study plotted with laboratory buffer layer spectra of Blakewell and Lumley ($y^+ = 20$, □) and Ueda and Hinze ($y^+ = 21$, •). Confidence limits not shown are the same as for the highest frequency estimate of our study.

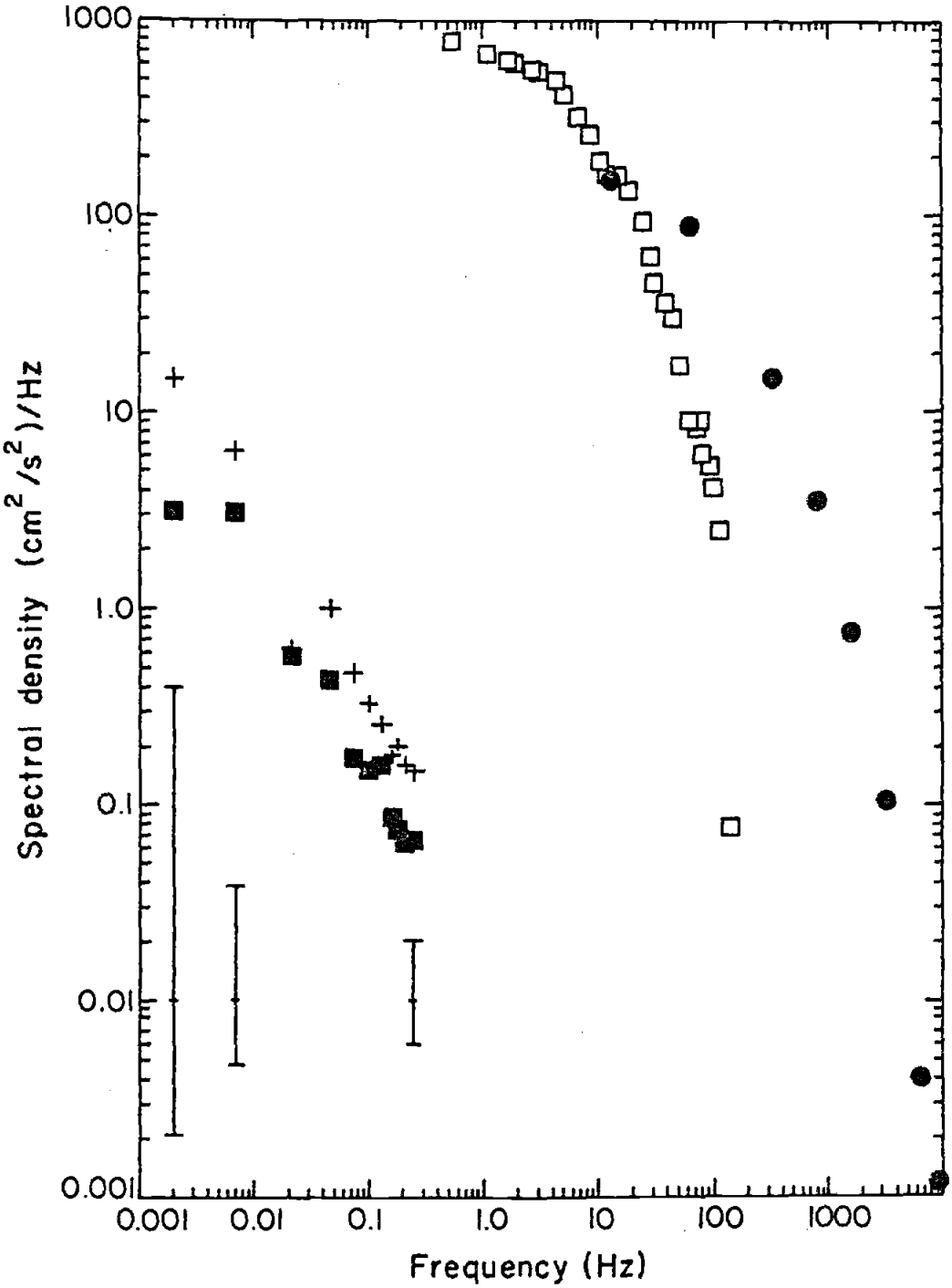
1000
100
10
1.0
0.1
0.01
0.001
Spectral density (cm²/s²)/Hz
0.001
0.01
0.1
1.0
10
100
1000
Frequency (Hz)

Figure III-8.

Figure III-9. Scaled versions of the laboratory buffer layer spectra shown in Figure III-8.

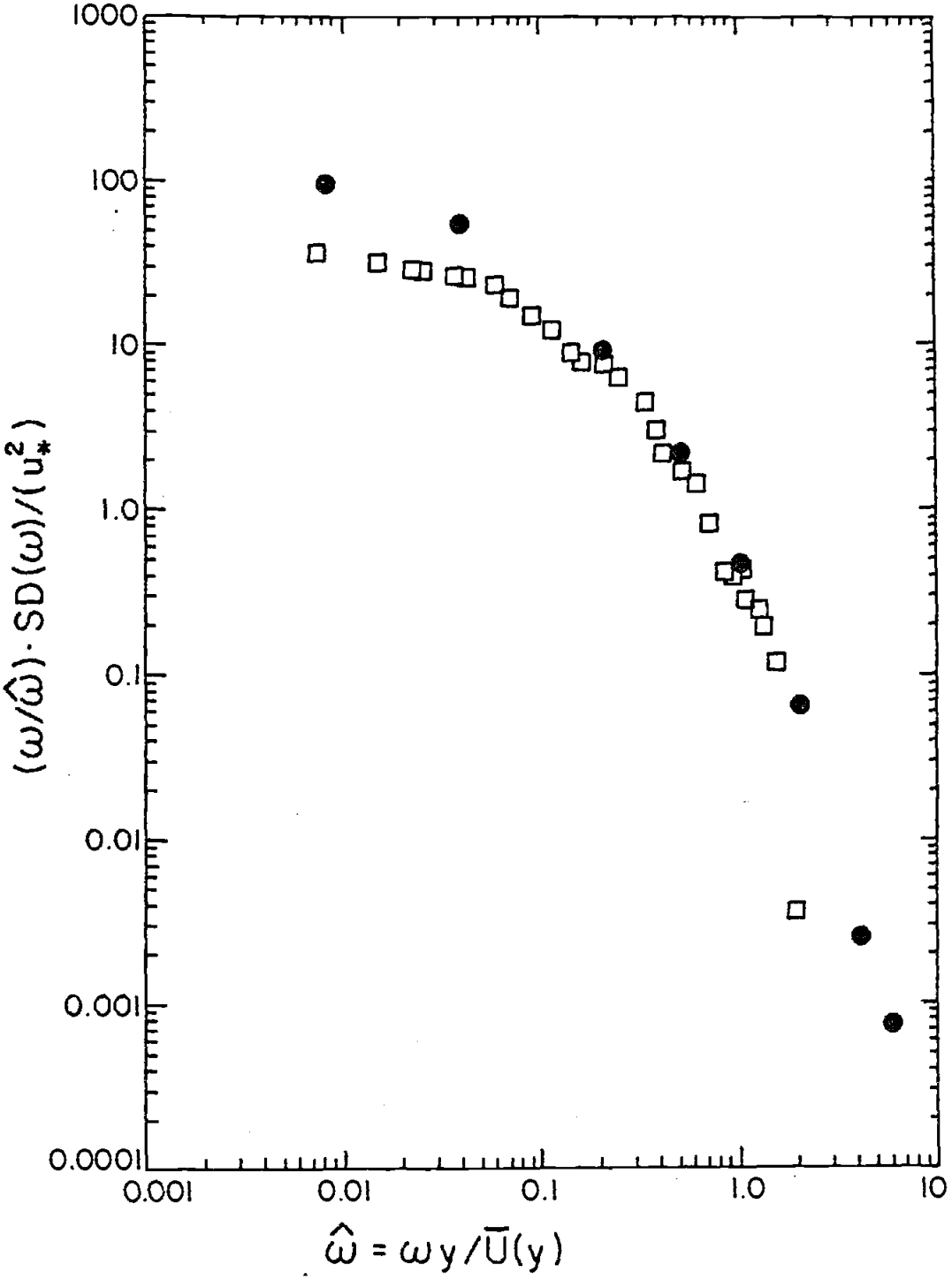
1000
100
10
1.0
0.1
0.01
0.001
0.0001
0.001
0.01
0.1
1.0
10
$(\omega/\hat{\omega})\cdot SD(\omega)/(u_*^2)$
$\hat{\omega} = \omega y/\bar{U}(y)$

Figure III-9.

scaled and unscaled spectra remain the same. Except for the lowest frequencies, the proposed scaling does collapse the laboratory data to a single curve. It should be noted that because the two sets of laboratory data have substantially the same y^+, we cannot argue that the proposed scaling is independent of y^+. Since the Reynolds numbers of the two laboratory experiments differed by a factor of 60, it appears that the scaling is indepedent of Reynolds number.

One difficulty in applying the proposed scaling to our data is that, because we cannot measure the shear in the sublayer when the sensors are in the buffer layer, we lack u_* measurements simultaneous to the buffer layer spectra. Stationary Savonius rotors on the platform indicate that the "mean" flow was not always constant between the time the sensors were in the sublayer and the time they were at the top of the profile. Thus, it is unreasonable to use u_* determinations from the sublayer to non-dimensionalize the buffer layer spectra. For lack of a better alternative, we have estimated u_* from the current speeds determined by the rotors located in the logarithmic layer. In doing so, we have assumed the commonly accepted value of 11.6 for the non-dimensional sublayer thickness (δ^+) even though data from an earlier study (Chriss and Caldwell, 1981b) indicate that δ^+ may vary from this value in the marine environment. (Because of the profiling scheme, determinations of δ^+ were not possible in the present study.) Chriss and Caldwell (1981b) show that u_* determinations based on log layer velocities and the assumption that $\delta^+ = 11.6$ may differ by as much as 30% from true u_* values (determined from sublayer data). Thus, using the rotors to estimate u_* must be

expected to introduce some error into the resulting non-dimensional spectra.

In Figure 10, we present scaled versions of our buffer layer spectra along with those from the two laboratory studies. Comparing with Figure 8, one can see that the scaling is relatively successful, particularly considering the potential uncertainties in the u_* estimates for our spectra. The shape of our ensemble-averaged spectrum (Fig. 11) is similar to those from the laboratory except that both ours and that of Ueda and Hinze (1975) show a slightly more extensive -1 power law range than does the spectrum of Blakewell and Lumley (1967).

7. Discussion

Although the proposed spectral scaling works reasonably well in both the viscous sublayer and the buffer layer, the spectra from the ocean floor fall below the laboratory spectra in the energy-containing portion of the non-dimensional frequency band (Figs. 7 and 11). (The horizontal arrows in these figures delimit the frequency band which contains 80% of the variance of the streamwise velocity fluctuations in the laboratory data.) Although the fact that our non-dimensional buffer-layer spectra fall below the laboratory spectra may be caused by inaccurate estimates of u_*, it is possible that the deviations from the laboratory spectra may reflect real differences in the flows.

Figure III-10. Scaled buffer layer spectra from our study plotted with those of the two laboratory studies. The laboratory spectra are shown with solid circles.

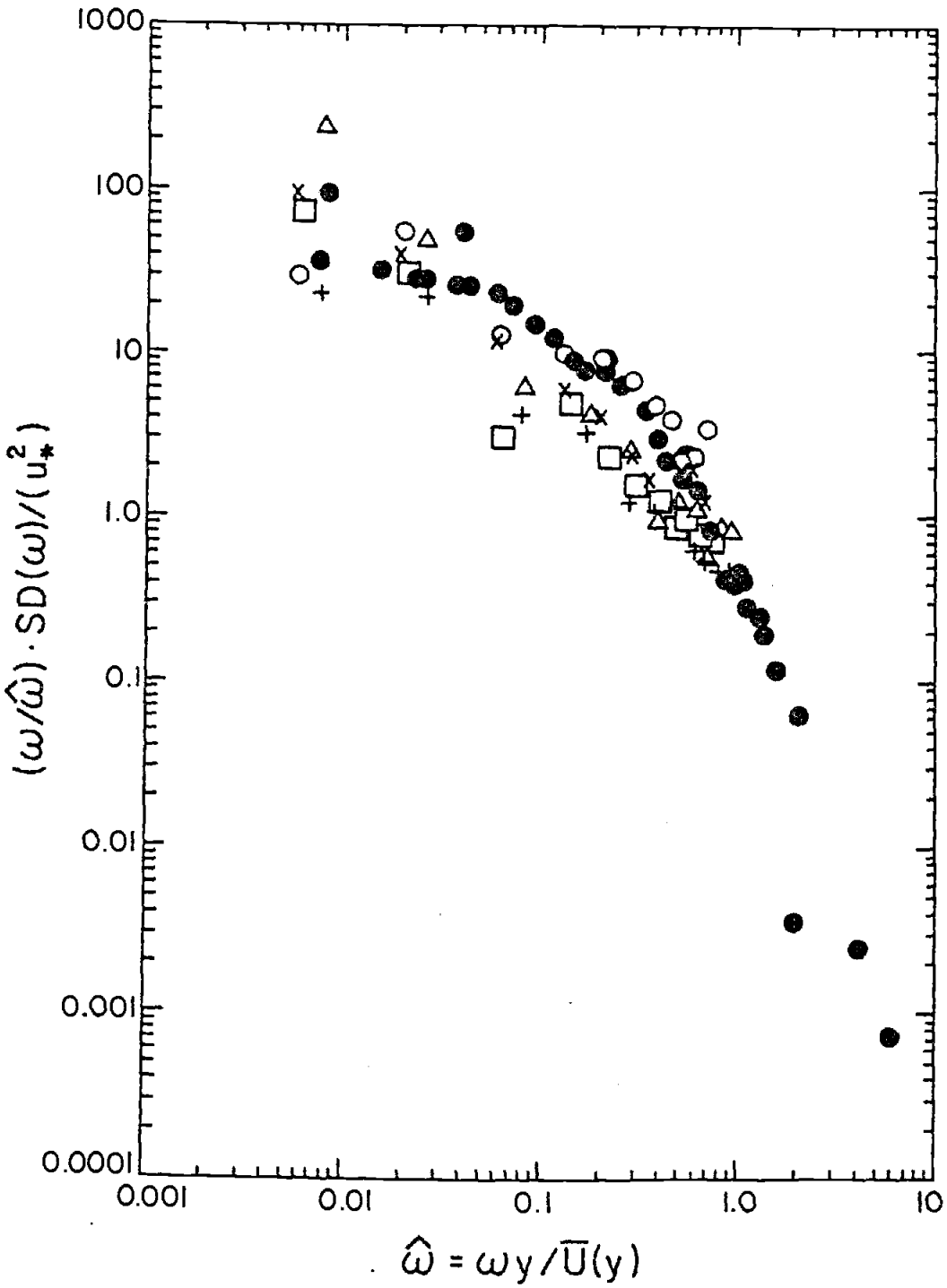

Figure III-10.

Figure III-11. Ensemble-averaged buffer layer spectrum from our study (■) plotted with laboratory buffer layer spectra (o). The horizontal arrows delimit the energy containing range of the laboratory spectra.

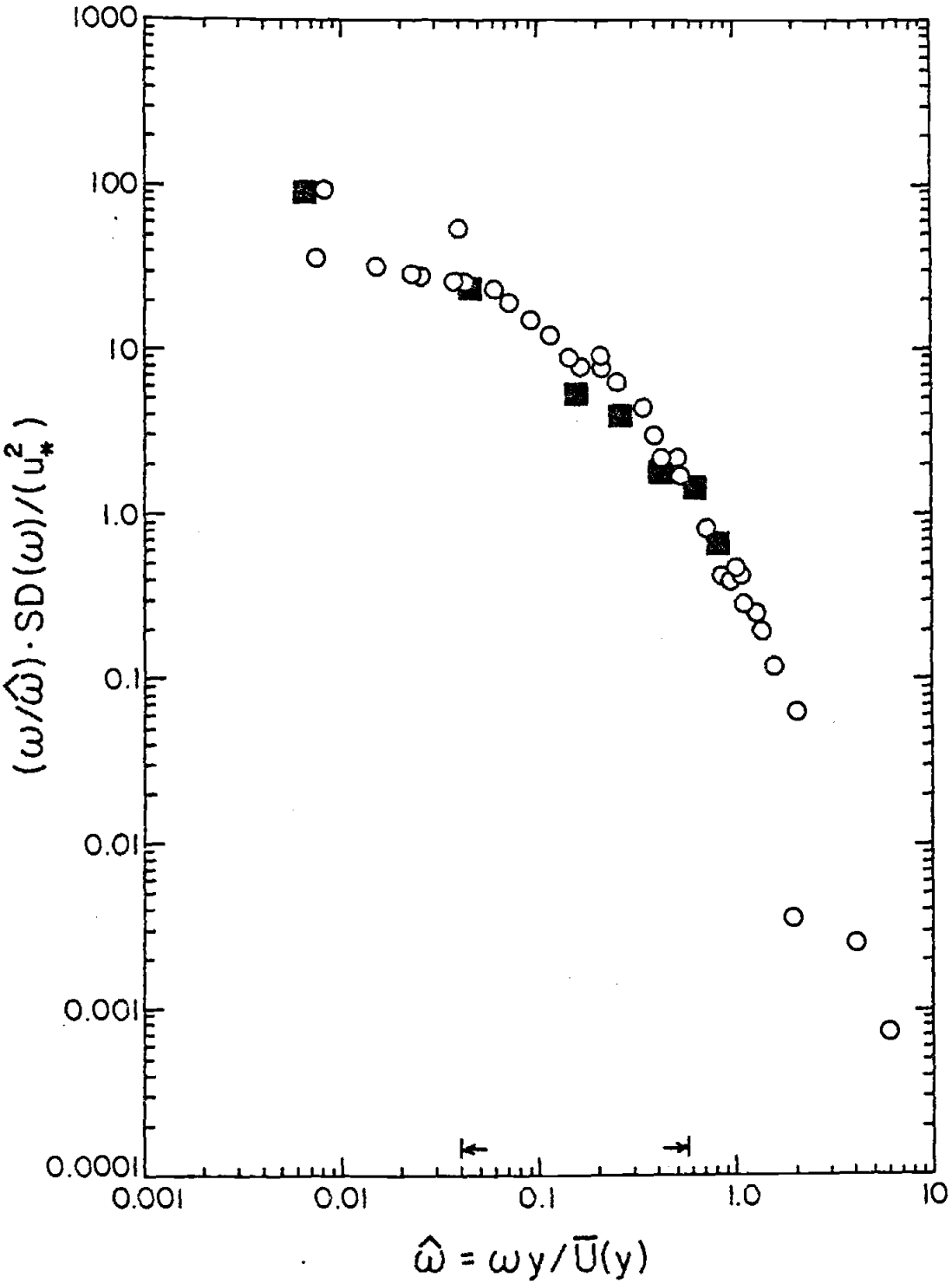

Figure III-11.

Based on laboratory studies of the "bursting" phenomena in smooth-walled turbulent boundary layer flows, Kim et al. (1971) and Zaric (1974) suggest that approximately 65% to 80% of the variance of the streamwise velocity fluctuations is contributed during "bursting" events and that the "quiescent" intervals between bursts contribute only 20% to 35% of the total variance. Rao et al. (1971) and Laufer and and Badri Narayanan (1971) discovered that, while the mean period between bursts, T_b, when scaled by ν/u_*^2 is strongly dependent on the boundary layer Reynolds number, a non-dimensional burst period, $T_b\ U_\infty/\delta$, based on the free stream velocity and the boundary layer thickness, δ, is not. Subsequent laboratory studies have confirmed this finding and indicate that the non-dimensional mean burst period ($T_b\ U_\infty/\delta$) is between 3 and 5 depending on the burst recognition criterion (Blackwelder and Kaplan, 1976; Wallace et al., 1977). The importance of these findings for spectral studies is that, to the extent that bursting influences u', the non-dimensional spectral density at a given non-dimensional frequency may differ in two boundary layer flows if the burst frequencies ($2\pi/T_b$) for the two flows occur at significantly different non-dimensional frequencies. Ueda and Hinze (1975) assume that the mean burst period is given by $T_b\ U_\infty/\delta = 4.7$ and note that, when non-dimensionalized by u_*^2/ν, the corresponding non-dimensional burst frequency is 0.027. A non-dimensional burst frequency of 0.1 can be estimated for the flow in the Blakewell and Lumley experiment if one takes the boundary layer thickness to be the pipe radius. Even though these estimates are not likely to be exact, it is important that, in both cases, the non-

dimensional frequency corresponding to the mean burst period falls within the energy containing band of the sublayer spectrum (Fig. 7).

While no data exists which demonstrates that bursting is important in the viscous sublayer of geophysical boundary layer flows, one can calculate the non-dimensional frequency which might be expected if bursting were important on the Oregon shelf. Because all of our current data were obtained within 1.5 m of the sea bed, it is not possible to determine the appropriate boundary layer thickness δ. However, taking the standard estimate of .4 u_*/f_c for the thickness of the Ekman layer (f_c is the Coriolis parameter), and estimating the free stream velocity as approximately 30 u_*, one obtains an estimate of 630 seconds for the mean burst period. The non-dimensional frequency ($\hat{\omega}_b = (2\pi\nu)/(u_*^2 T_b)$) corresponding to this period ranges from 0.001 to 0.006 for the measured range of u_* in our experiment. If the sublayer burst period in large-scale geophysical flows scales with that of laboratory flows, and if the Ekman depth is the relevant boundary layer thickness, the non-dimensional burst frequency for our data would lie considerably outside the energy containing range for the laboratory spectra (Fig. 7). If one assumes that the Ekman depth is not the relevant boundary layer thickness, one can determine what boundary layer thickness would be required to have the same non-dimensional burst frequency (0.027) as in Ueda and Hinze's study. These calculated thicknesses range from 62 cm (at $u_* = 0.36$) to 149 cm (at $u_* = 0.15$) and are unreasonably small for the bottom boundary layer on the shelf. This simple exercise suggests that, if bursting is important in the sublayer on the continental shelf, and

if $T_b U_\infty/\delta = 4.7$, the non-dimensional frequency corresponding to mean burst period is very different from that of laboratory experiments and is outside the energy containing range of the laboratory spectra. This frequency, in fact, would be nearly at the low frequency limit of the spectra in Figure 7. The agreement between our sublayer spectra and the laboratory spectra at the lowest non-dimensional frequencies might be taken to indicate that bursting did not contribute to u' at these frequencies during our study. However, this conclusion is not warranted because of the removal of low frequency energy by the detrending necessary to remove the effect of the mean shear in the sublayer. Although the profiler motion in the sublayer prevents an accurate comparison of the geophysical and laboratory spectra at very low non-dimensional frequencies, we were able to compute spectra for two 1024-point buffer layer series during which the mean flow was relatively steady. Although the larger amount of low frequency energy (compared with laboratory spectra, Fig. 12) is consistent with what might be expected if geophysical sublayer bursting obeys the same scaling as in laboratory flows, energy at these time scales (7 to 22 minutes) could equally well be contributed by a number of processes (internal waves, low frequency turbulence, etc.) completely unrelated to bursting. The determination of whether bursting is significant in geophysical sublayers must await the development of Reynolds stress sensors capable of operating in the sublayer and buffer layer of geophysical flows.

Figure III-12. Buffer layer spectra for the two 1024-point series (solid symbols) plotted with the laboratory spectra (o). Confidence intervals shown are for our data.

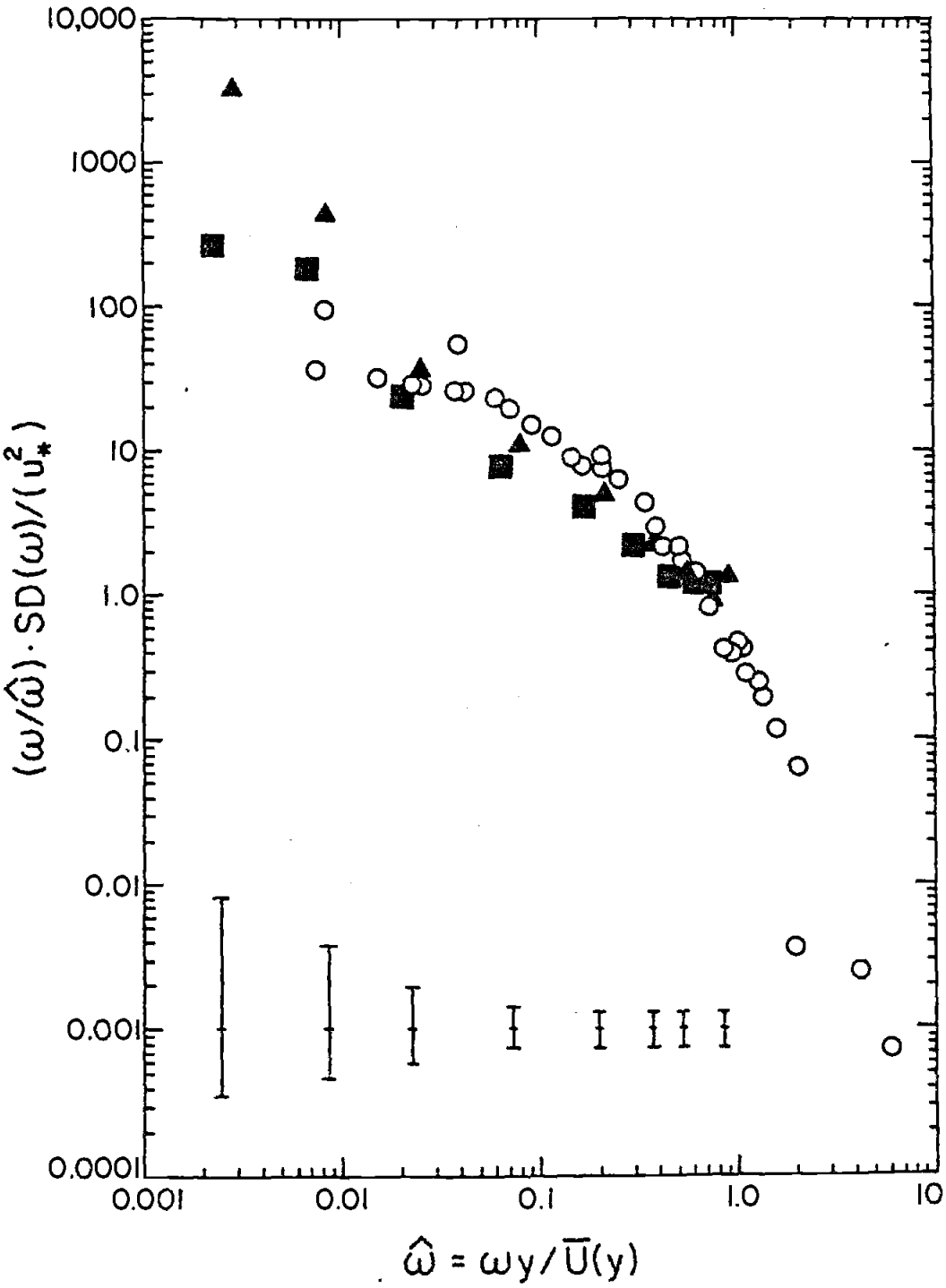

Figure III-12.

8. Conclusions

Spectra of velocity fluctuations have been determined for the first time in the viscous sublayer and buffer layer of a geophysical boundary layer flow. The spectral scaling proposed by Blakewell and Lumley (1967) for the viscous sublayer works remarkably well in collapsing the sublayer spectra from this geophysical and several different laboratory flows. Buffer layer spectra from $y^+ = 18$ to $y^+ = 29$ collapse reasonably well with laboratory spectra ($y^+ \simeq 20$) when frequencies are scaled by $\bar{U}(y)/y$ and spectral densities are scaled by $u_*^2 \hat{\omega}/\omega$, where $\hat{\omega}$ is the non-dimensional frequency given by $\omega y/\bar{U}(y)$.

Although this scaling is moderately effective, the non-dimensional spectral densities of the geophysical sublayer and buffer layer spectra fall slightly below the laboratory spectra in the energy-containing portion of the frequency band. This observation may be related to the fact that, if the sublayer burst period for geophysical flows scales according to laboratory results, the corresponding non-dimensional burst frequency for the geophysical flow may lie outside the energy-containing range of the non-dimensional laboratory spectra.

Geophysical boundary layer experiments must be conducted in which Reynolds stress sensors remain fixed at one position in the viscous sublayer for a sufficiently long time in order to resolve the low frequency portion of the spectrum where the effects of the bursting phenomena may be apparent.

REFERENCES

Arya, S. P. S., Contribution of form drag on pressure ridges to the air stress on arctic ice, J. Geophys. Res., 78,7092-7099, 1973.

Arya, S. P. S., A drag partition theory for determining the large-scale roughness parameter and wind stress on the arctic pack ice, J. Geophys. Res., 80,3447-3454, 1975a.

Arya, S. P. S., Buoyancy effects in a horizontal flat-plate boundary layer, J. Fluid Mech., 68,321-343, 1975b.

Badgley, F. I., Paulson, C. A. and Miyake, M., Profiles of Wind, Temperature, and Humidity over the Arabian Sea, p. 42, University of Hawaii Press, 1972.

Bath, M., Spectral Analysis in Geophysics, 563 pp. Elsevier Scientific Publishing Company, Amsterdam, 1974.

Blackwelder, R. F. and R. E. Kaplan, On the wall structure of the turbulent boundary layer, J. Fluid Mech., 76,89-112, 1976.

Blakewell, H. P. and J. L. Lumley, Viscous sublayer and adjacent wall region in turbulent pipe flow, Phys. Fluids, 10,1880-1889, 1967.

Bowden, K. F., Physical problems of the benthic boundary layer, Geophysical Surveys, 3,255-296, 1978.

Bradley, E. F., A micrometeorological study of velocity profiles and surface drag in the region modified by a change in surface roughness, Quart. J. Roy. Meteorological Soc., 94,361-379, 1968.

Caldwell, D. R., C. W. Van Atta and K. N. Helland, A laboratory study of the turbulent Ekman layer, Geophys. Fluid Dyn., 3,125-160, 1972.

Caldwell, D. R., Variability of the bottom mixed layer on the Oregon shelf, Deep-Sea Res., 25,1235-1244, 1978.

Caldwell, D. R. and T. M. Chriss, The viscous sublayer at the sea floor, Science, 205,1131-1132, 1979.

Chriss, T. M. and D. R. Caldwell, Evidence for the influence of form drag on bottom boundary layer flow, J. Geophys. Res. (under revision), 1981a.

Chriss, T. M. and D. R. Caldwell, Universal similarity and the thickness of the viscous sublayer at the ocean floor, J. Geophys. Res. (submitted), 1981b.

Csanady, G. T., The "roughness" of the sea surface in light winds, J. Geophys. Res., 79,2747-2751, 1974.

Csanady, G. T., Turbulent interface layers, J. Geophys. Res., 83,2329-2342, 1978.

Dillon, T. M. and D. R. Caldwell, The Batchelor spectrum and dissipation in the upper ocean, J. Geophys. Res., 85,1910-1916, 1980.

Draper, N. R. and H. Smith, Applied Regression Analysis, 407 pp., John Wiley and Sons, Inc., 1966.

Eckelmann, H., The structure of the viscous sublayer and the adjacent wall region in a turbulent channel flow, J. Fluid Mech., 65,439-459, 1974.

Elliot, W. P., The growth of the atmospheric internal boundary layer, Eos Trans. AGU, 39,1048-1054, 1958.

Fortuna, G. and T. J. Hanratty, Frequency response of the boundary layer on wall transfer probes, Int. J. Heat Mass Transfer, 14,1499-1507, 1971.

Garrett, J. R., Review of drag coefficients over oceans and continents, Mon. Wea. Rev., 105,915-929, 1977.

Gordon, C. M., Sediment entrainment and suspension in a turbulent tidal flow, Mar. Geol., 18,M57-M64, 1975.

Gust, G., Observations on turbulent-drag reduction in a dilute suspension of clay in sea-water, J. Fluid Mech., 75,29-47, 1976.

Hanratty, T. J., Study of turbulence close to a solid wall, Phys. Fluids Suppl., 10,S126-S133, 1967.

Hanratty, T. J., L. G. Chorn and D. T. Hatziavramidis, Turbulent fluctuations in the viscous wall region for Newtonian and drag reducing fluids, Phys. Fluids, 20,S112-S119, 1977.

Kim, H. T., S. J. Kline and W. C. Reynolds, The production of turbulence near a smooth wall in a turbulent boundary layer, J. Fluid Mech., 50,133-160, 1971.

Klebanoff, P. S., Characteristics in a boundary layer with zero pressure gradient, NACA TN 3187, 1954.

Komar, P. D., Boundary layer flow under steady unidirectional currents, in Marine Sediment Transport and Environmental Management, edited by D. J. Standley and D. J. P. Swift, John Wiley and Sons, New York, NY, 1976.

Komar, P. D., R. H. Neudeck and L. D. Kulm, Observations and significance of deep-water oscillatory ripple marks on the Oregon continental shelf, in Shelf Sediment Transport, edited by D. J. P. Swift, D. B. Duane and O. H. Pilkey, p. 601-619, Dowden, Hutchinson and Ross, Stroudsberg, PA, 1972.

Kreplin, H.-P. and H. Eckelmann, Behavior of the three fluctuating components in the wall region of a turbulent channel flow, Phys. Fluids, 22,1233-1239, 1979.

Laufer, J., Investigation of turbulent flow in a two-dimensional channel, NACA TR 1053, 1951.

Laufer, J., The structure of turbulence in fully developed pipe flow, NACA TR 1174, 1954.

Laufer, J. and M. A. Badri Narayanan, Mean period of the turbulent production mechanism in a boundary layer, Phys. Fluids, 14,182-183, 1971.

Ludwick, J. C., Variations in boundary drag coefficient in the tidal entrance to Chesapeake Bay, Virginia, Mar. Geol., 19,19-28, 1975.

McCave, I. N., Some boundary-layer characteristics of tidal currents bearing sand in suspension, Mém. Soc. Roy. Sci. Liège, 6^{e} Série, 6,107-126, 1973.

Miller, M. C. and P. D. Komar, Oscillation sand ripples generated by laboratory apparatus, J. Sed. Petrology, 50,173-182, 1980.

Mitchell, J. E. and T. J. Hanratty, A study of turbulence at the wall using an electrochemical wall shear-stress meter, J. Fluid Mech., 26,199-221, 1966.

Monin, A. S. and A. M. Yaglom, Statistical Fluid Mechanics, 769 pp., MIT Press, Cambridge, MA, 1971.

Newberger, P. A. and D. R. Caldwell, Mixing and the bottom nepheloid layer, Mar. Geol., 41,321-336, 1981.

Paola, C., G. Gust and J. Southard, Flow structure and skin friction over two-dimensional ripples (abstract), Eos Trans. AGU, 61,989-990, 1980.

Portman, D. J., An improved technique for measuring wind and temperature profiles over water and some results obtained for light winds, Publ. 4, pp. 77-84, Great Lakes Res. Div., Univ. of Mich., Ann Arbor, 1960.

Py, B., Etude tridimensionnelle de la sous-couche visqueuse dans une veine rectangulaire par des mesures de transfert de matiere en paroi, Int. J. Heat Mass Transfer, 16,129-144, 1973.

Rao, K., R. Narasimha and M. A. Badri Narayanan, The 'bursting' phenomenon in a turbulent boundary layer, J. Fluid Mech., 48,339-352, 1971.

Rao, K. S., J. C. Wyngaard and O. R. Coté, The structure of the two-dimensional internal boundary layer over a sudden change of surface roughness, J. Atmos. Sci., 31,738-746, 1974.

Runge, E. J., Continental shelf sediments, Columbia River to Cape Blanco, Oregon, Ph.D. thesis, Oregon State Univ., Corvallis, 1966.

Sheppard, P. A., D. T. Tribble and J. R. Garrett, Studies of turbulence in the surface layer over water, Quart. J. Roy. Meteorol. Soc., 98,627-641, 1972.

Smith, J. D., Modeling of sediment transport on continental shelves, in The Sea, vol. 6, edited by E. D. Goldberg, John Wiley, New York, NY, 1977.

Smith, J. D. and S. R. McLean, Spatially averaged flow over a wavy surface, J. Geophys. Res., 82,1735-1746, 1977.

Sreenivasan, K. R. and R. A. Antonia, Properties of wall shear stress fluctuations in a turbulent duct flow, J. Appl. Mech., 44,389-395, 1977.

Sternberg, R. W., Friction factors in tidal channels with differing bed roughness, Mar. Geol., 6,243-260, 1968.

Sternberg, R. W., Predicting initial motion and bedload transport of sediment particles in the shallow marine environment, in Shelf Sediment Transport, edited by D. J. P. Swift, D. B. Duane and O. H. Pilkey, p. 61-82, Dowden, Hutchinson and Ross, Stroudsberg, PA, 1972.

Townsend, A. A., The Structure of Turbulent Shear Flow, 429 pp., Cambridge University Press, London, 1976.

Ueda, H. and J. O. Hinze, Fine-structure turbulence in the wall region of a turbulent boundary layer, J. Fluid Mech., 67,125-143, 1975.

Wallace, J. M., R. S. Brodkey and H. Eckelmann, Pattern-recognized structures in bounded turbulent shear flows, J. Fluid Mech., 83,673-693, 1977.

Weatherly, G. L. and M. Wimbush, Near-bottom speed and temperature observations on the Blake-Bahama Outer Ridge, J. Geophys. Res., 85,3971-3981, 1980.

Wimbush, M. and W. Munk, The benthic boundary layer, in The Sea, Vol. 4, Part 1, edited by A. E. Maxwell, p. 731-758, Wiley-Interscience, New York, 1971.

Yaglom, A. M., Similarity laws for constant-pressure and pressure-gradient turbulent wall flows, Ann. Rev. Fluid Mech., 11,505-540, 1979.

Zaric, Z., Statistical analysis of wall turbulence phenomena, in Turbulent Diffusion in Environmental Pollution, edited by F. N. Frenkiel and R. E. Munn, Adv. in Geophysics, 18a,249-261, Academic Press, New York, 1974.